NASA Technical Paper 2653

January 1987

Applicability of Linearized-Theory Attached-Flow Methods to Design and Analysis of Flap Systems at Low Speeds for Thin Swept Wings With Sharp Leading Edges

Harry W. Carlson and
Christine M. Darden

NASA

NASA Technical Paper 2653

1987

Applicability of Linearized-Theory Attached-Flow Methods to Design and Analysis of Flap Systems at Low Speeds for Thin Swept Wings With Sharp Leading Edges

Harry W. Carlson
PRC Kentron, Inc.
Hampton, Virginia

Christine M. Darden
Langley Research Center
Hampton, Virginia

NASA
National Aeronautics and Space Administration

Scientific and Technical Information Branch

Summary

Low-speed experimental force data on a series of thin swept wings with sharp leading edges and leading- and trailing-edge flaps are compared with predictions made using a linearized-theory method which includes estimates of vortex forces. These comparisons were made to assess the effectiveness of linearized-theory methods for use in the design and analysis of flap systems in subsonic flow. Results demonstrate that linearized-theory, attached-flow methods (with approximate representation of vortex forces) can form the basis of a rational system for flap design and analysis. Even attached-flow methods that do not take vortex forces into account can be used for the selection of optimized flap-system geometry, but design-point performance levels tend to be underestimated unless vortex forces are included. Illustrative examples of the use of these methods in the design of efficient low-speed flap systems are included.

Introduction

A study of the use of linearized-theory methods for the design and analysis of simple low-speed flap systems is presented in reference 1. The application of the methods to the special case of sharp leading-edge flaps was considered in reference 2. The underlying premise of these studies was that high levels of aerodynamic performance for any flap system can be achieved only if the flow about the wing remains predominantly attached. Because of the implied need for criteria to judge the degree of flow attachment, a better statement of the premise would be that the highest achievable levels of flap-system aerodynamic performance require a flow that is as nearly attached as circumstances allow. Simple hinged leading-edge flaps with sharp leading edges prevent the attainment of attached flow because of the separation that occurs at either the leading edge or the hinge line. However, the selection of flap geometry to provide a reasonable division of flow turning between that which occurs at the leading edge and that which occurs at the hinge line helps minimize the overall extent of flow separation. Also, the use of trailing-edge flap deflection to reduce the wing angle of attack for a given lift serves to reduce the necessary flow turning over the forward portion of the wing and further aids in the goal of providing an approach to attached flow. References 1 and 2 illustrate how an attached-flow wing-design method (ref. 3) can be used in the selection of candidate flap systems to approximate attached-flow surfaces and loadings and how an attached-flow flap-system evaluation method (ref. 4) can be used to estimate achievable performance levels.

A limited validation of the design procedure with correlations of theoretical and experimental data was presented in references 1 and 2. In previous studies (refs. 5 and 6), an attached-flow camber surface was used as a point of departure, and that surface was then modified to create a small detached leading-edge vortex force for optimization of aerodynamic performance in separated flow. These studies show good aerodynamic performance and good agreement between experiment and vortex-flow modified linearized theory. Nevertheless, there is a need for a more complete exploration of the applicability and limitations of linearized-theory attached-flow methods to the design and analysis of low-speed flap systems. For that purpose, the present paper utilizes a relatively complete set of experimental force data for a series of thin swept wings with leading- and trailing-edge flaps. (See ref. 7.) Extensive correlations of theoretical and experimental results are used to illustrate the relatively good agreement for flap settings which result in good performance and the poor agreement for flap settings far from optimum values. The study also shows, in some detail, the variation of optimum leading-edge and trailing-edge flap deflections with lift coefficient as well as the ability of attached-flow methods to predict these settings and the resultant performance levels.

Symbols

AR	wing aspect ratio, b^2/S
b	wing span, in.
C_A	wing axial- or chord-force coefficient
C_D	wing drag coefficient
ΔC_D	drag coefficient due to lift, $C_D - C_{D,o}$
$C_{D,o}$	drag coefficient at $\alpha = 0°$ for a wing with no camber or twist
C_L	wing lift coefficient
$C_{L,\text{des}}$	wing design lift coefficient
$C_{L,\alpha}$	wing lift curve slope at $\alpha = 0°$, per deg
C_m	wing pitching-moment coefficient
$C_{m,\text{des}}$	wing design pitching-moment coefficient
C_N	wing normal-force coefficient
ΔC_p	lifting-pressure coefficient
$\bar{c}$	mean aerodynamic chord, in.
c_L	leading-edge flap chord, in.

c_r	wing root chord, in.
c_T	trailing-edge flap chord, in.
S	wing reference area, in^2
S_s	suction parameter, $\frac{C_L \tan(C_L/C_{L,\alpha}) - \Delta C_D}{C_L \tan(C_L/C_{L,\alpha}) - C_L^2/(\pi \mathrm{AR})}$
$S_{s,\max}$	maximum suction parameter achieved when both leading-edge flap deflection and trailing-edge flap deflection are free to change
$S_{s,\max,L}$	maximum suction parameter achieved when leading-edge flap deflection is free to change, but trailing-edge flap deflection is held at a fixed value
x, y, z	Cartesian coordinates
x'	distance in x-direction measured from wing leading edge
α	wing angle of attack, deg
$\delta_{L,n}$	leading-edge flap deflection angle measured normal to hinge line, positive with leading edge down, deg
$\delta_{L,n,\mathrm{opt}}$	value of $\delta_{L,n}$ at which $S_{s,\max,L}$ is achieved
$\delta_{L,s}$	leading-edge flap streamwise deflection angle, positive with leading edge down, deg
$\delta_{T,n}$	trailing-edge flap deflection angle measured normal to hinge line, positive with trailing edge down, deg
$\delta_{T,n,\mathrm{opt}}$	value of $\delta_{T,n}$ at which $S_{s,\max}$ is achieved
$\delta_{T,s}$	trailing-edge flap streamwise deflection angle, positive with trailing edge down, deg

Flap Design and Analysis Methodology

The flap design and analysis concepts originally presented in references 1 and 2 are based on the assumption that only through an approach to attached-flow conditions can wing performance be maximized. Thus, under circumstances in which flow separation is unavoidable, that separation should be reduced and locally confined insofar as possible. To begin a brief review of these concepts, consider the twisted and cambered wing section shown in sketch A. Wing sections such as this are employed to avoid flow separation that occurs at the leading edge of thin, flat wing surfaces and prevents the achievement of theoretical leading-edge thrust. A distributed thrust over the forward portion of the curved wing section replaces the flat-surface, concentrated, theoretical leading-edge thrust and offers comparable aerodynamic efficiency. The gently curved surface and the more nearly uniform lifting pressure distribution (compared with the flat-surface distribution with its leading-edge singularity) helps to avoid flow separation that occurs when sharp changes in flow direction are encountered. The dependence of the onset of flow separation on Mach number, Reynolds number, and other possible factors is not fully understood, but it is clear, as shown in reference 4, that high Mach numbers and low Reynolds numbers decrease the possibilities of fully attached flow. Increased design lift coefficients also increase the severity of the problem.

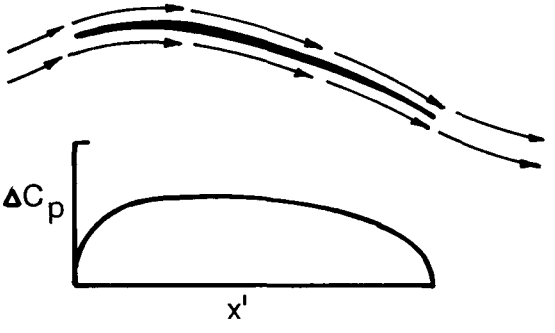

Sketch A

When the designer is not free to choose a continuously curved surface, but must rely on simple hinged flaps, the problem becomes more complex. As shown in sketch B, for an airfoil composed of connected straight-line segments, theoretical singularities cannot be avoided. Singularities will appear at the leading edge and/or the leading-edge flap hinge line—generally both. The airfoil section shown also employs a trailing-edge flap to reduce the wing angle of attack required for a given lift coefficient and to reduce the requirement for flow turning at the leading edge and at the leading-edge flap hinge line. The trailing-edge flap hinge line introduces a third theoretical singularity; however, for reasons discussed in references 1 and 2, flow separation associated with this singularity is not nearly as detrimental to wing aerodynamic performance as separation in the leading-edge flap region.

With no leading-edge flap deflection, as shown at the top of sketch B, a strong theoretical flat-wing leading-edge singularity develops. But, of course,

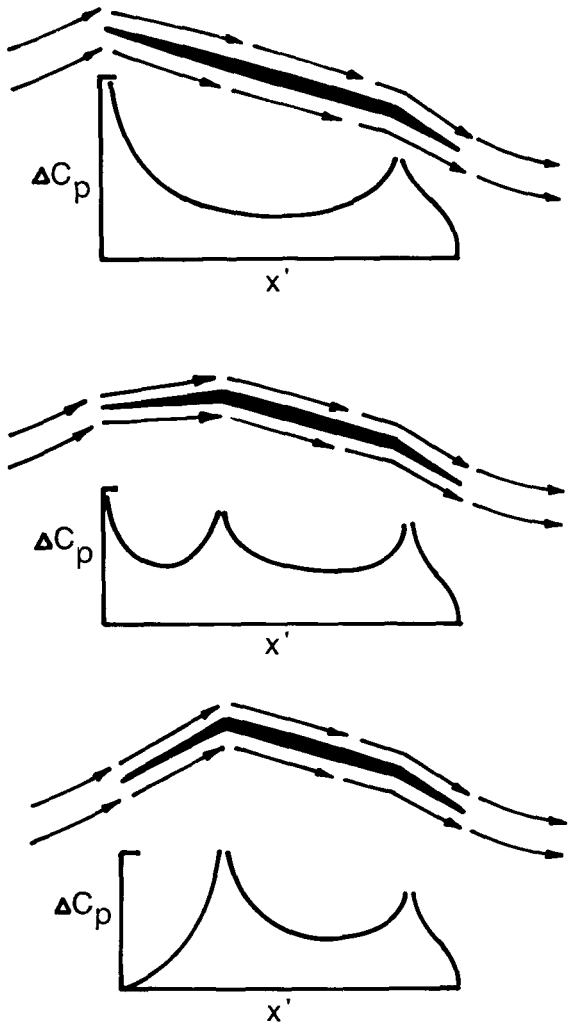

Sketch B

there will be no leading-edge flap hinge-line singularity. For that airfoil section, flow separation at the leading edge is unavoidable, and the loss of the theoretical leading-edge thrust brings about severe performance penalties.

If, as shown at the bottom of sketch B, the leading-edge flap is deflected enough to bring about a smooth local onflow at the leading edge (an alignment of the local upwash field and the flap surface), the leading-edge singularity and the resultant leading-edge separation can be avoided. However, for such a severe deflection, the theoretical attached-flow solution would show a performance penalty relative to that of an optimum deflection. (See ref. 1.) Furthermore, the performance of this flap depends on the loading in the vicinity of the hinge line which may not be achievable. The hinge-line singularity, which would be comparable in strength to the undeflected flap leading-edge singularity, would in all probability induce a local flow separation and cause a further performance loss.

The compromise leading-edge flap deflection shown in the middle of sketch B is intended to approximate, as closely as possible, the camber surface and pressure distribution of a well-designed wing surface such as that shown in sketch A. For this airfoil section, theoretical pressure singularities appear at both the leading edge and hinge line. The leading-edge singularity is of reduced strength compared with that of a flat wing, but it is not reduced to zero as in the case of the well-designed camber surface or the fully deflected leading-edge flap. Thus, there remains some theoretical leading-edge thrust, which together with distributed thrust over the leading-edge flap surface, preserves good theoretical attached-flow performance comparable to that of the flat wing with full theoretical leading-edge thrust. It is anticipated that a reasonable division of singularity strength between the leading edge and the hinge line would reduce the flow separation tendencies and the resultant performance penalties.

The actual flow about a deflected-flap airfoil approximating a well-designed camber surface can be quite different from the flow depicted in the middle of sketch B. With a sharp leading-edge airfoil, the leading-edge singularity would not develop, and the theoretical leading-edge thrust would be converted to a vortex force according to the Polhamus analogy. (See ref. 8.) A flow field similar to that shown in sketch C would be expected to form. The boundary layer separates from the surface at the leading edge and encloses a region of circulation whose strength is related to the theoretical leading-edge thrust. Because the theoretical thrust for the deflected leading-edge flap is relatively small (compared with the theoretical thrust for the flat wing), the vortex force associated with the circulation within the separated region is also relatively small.

The relationship between separated and theoretical attached flow for efficient flap systems may be further explored with the aid of sketch D. The dashed line represents the mean camber surface of a flap-system airfoil section and the corresponding theoretical attached-flow lifting-pressure distribution. For the same section in separated flow, most of the force distribution (excluding the vortex force) is caused by the flow external to the separated region, a flow described by a streamline which emanates from the wing leading edge and reattaches on the wing upper surface. The short-dash–long-dash line represents an effective mean-camber surface for the separated flow and the corresponding lifting-pressure distribution.

If, as shown at the bottom of sketch D, the separated flow returns to the surface in the vicinity of the

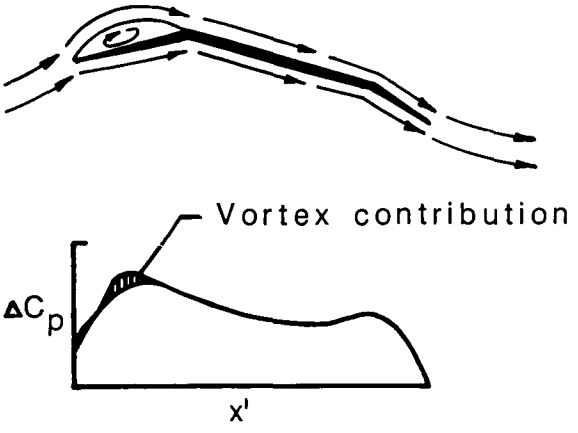

Sketch C

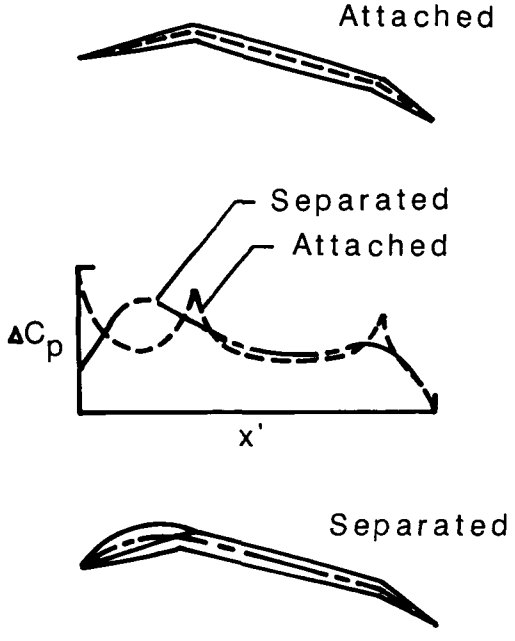

Sketch D

leading-edge flap hinge line, the efficiency of the system is close to that of the fully attached flow depicted at the top of the sketch. This can happen because the change of downward momentum of the flow over the flap itself is approximately the same for separated and attached flow; therefore, the lifting force is approximately the same. The distribution of this force over the flap is different from the attached flow, perhaps as shown in the pressure distribution of the sketch; however, because of the uniform slope of the flap surface, the integrated force in separated and attached flow is approximately the same. Thus, for reasonably efficient flap systems, the attached-flow solution can model the forces generated in the actual separated flow, even though the attached and separated flow fields have entirely different structures.

When the vortex force associated with circulation within the separated region is taken into account, the total loading on the flap is somewhat larger for separated flow than for attached. Thus, there is no loss in lifting efficiency for the separated flow relative to the attached flow, except for the exchange of the theoretical thrust for the less-efficient vortex force. As discussed in reference 1, the attached-flow solution can also model the vortex contribution to the pressure distribution by using the Polhamus analogy and deleting the leading-edge thrust term.

The flow depicted in sketch C and at the bottom of sketch D is considered to be predominantly attached because, to a large extent, the flow patterns are as close to attached-flow patterns as circumstances (sharp leading edges and sharp hinge lines) allow, and the performance level should be close to that achievable with attached flow. The principle of seeking reattachment at the hinge line in the design of sharp leading-edge flaps was originally discussed by Rao in reference 9 and was verified experimentally by Frink in reference 10. In a subsequent section of this report, experimental data are used in an assessment of the sensitivity of flap-system aerodynamic performance, and the associated flow separation and reattachment, to leading-edge flap deflection. Although double-hinged flaps selected to approximate an efficient camber surface design could be handled by the present method and would be expected to offer improved performance relative to the single-hinged flaps, that additional complexity is beyond the scope of the present study. Performance benefits that would arise from rounding of the wing leading edge are also excluded to keep the focus of the study on problems associated with thin, sharp leading-edge wings.

Sharp leading-edge wing-flap systems intended to produce reattachment of the separated leading-edge vortex at the leading-edge flap hinge line as described in the preceding paragraph are commonly called "vortex flaps." This name, because it may imply the deliberate creation of a powerful vortex force, can be misleading to the uninitiated. Descriptions of the concept sometimes encourage this interpretation. For example, in reference 9 the author states, "This paper presents a new concept, the 'vortex flap', which aims to exploit rather than suppress the natural tendency towards flow separation and vortex formation at highly swept leading edges, and thus offers a more rational approach to flow management for improved subsonic efficiency of slender wings at high angles of attack." Reference 10 more correctly refers to a

"small vortex over the flap" whose purpose is to "promote flow reattachment along the hinge line." The goal of vortex flap design is actually the same as that for the design of any efficient lifting system—to approach a predominantly attached flow condition as closely as circumstances allow.

The foregoing considerations led to the hypothesis that flow patterns as close to those of attached flow as circumstances allow are required for good flap-system performance and that linearized-theory attached-flow methods (with separated vortices taken into account by means of the suction analogy) are well suited to the design and analysis of efficient flaps. The study of the validity of the concepts initiated in references 1 and 2 has been extended in this paper to cover a wider range of planforms and a wider range of lift coefficients.

The wing-design method of reference 6 has a fundamental similarity to the design approach discussed in reference 1 and in this report, but there are some significant differences. Both approaches begin with a linearized-theory attached-flow solution for an optimized wing camber surface and modify that surface in an attempt to achieve high levels of aerodynamic efficiency under constraints imposed by actual flight conditions and design limitations. The study of reference 6, however, dealt with the selection of a modified wing camber surface for a design Mach number of 0.9 rather than with the selection flap surfaces for low speeds. The two approaches also differ in the detailed steps used in the derivation of the modified surface.

Vortex flap design methods based on the concept introduced in reference 9 differ from the present approach primarily in the use of wing analysis methods in an iterative manner to define the required flap chords and deflections. This iterative process allows the definition of leading edges which are curved in planform so as to promote flow reattachment at the straight hinge line of single-segment leading-edge flaps. The present approach is tailored to the direct design of segmented leading-edge flaps acting in combination with trailing-edge flaps. Single-segment leading-edge flaps can also be treated as described in reference 1. The design of curved leading edges by using the present approach would require an iterative process.

Evaluation of Flap System Performance

The comparisons of theory and experiment used in this paper to validate the concepts are restricted to force data. This is believed to be sufficient because the simple nature of the surface slope distribution for the wings of this study and the analysis of the data through the use of axial- and normal-force coefficients allows a piece-by-piece study of the factors contributing to aerodynamic efficiency. A sufficient proof of the concept is believed to be a demonstration of the ability of computational methods employing the previously described accounting techniques to predict the performance of reasonably efficient flap systems.

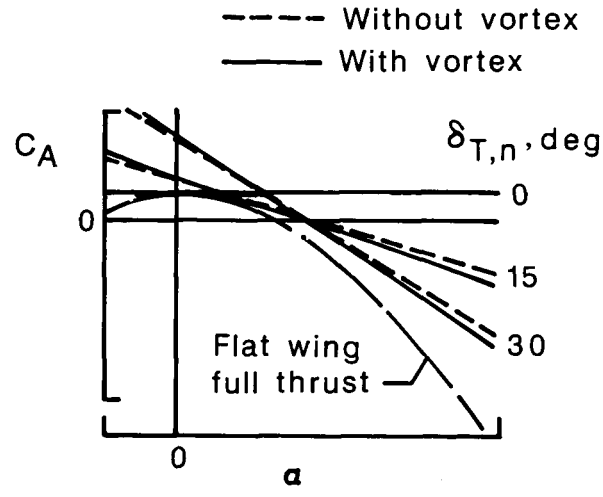

Sketch E

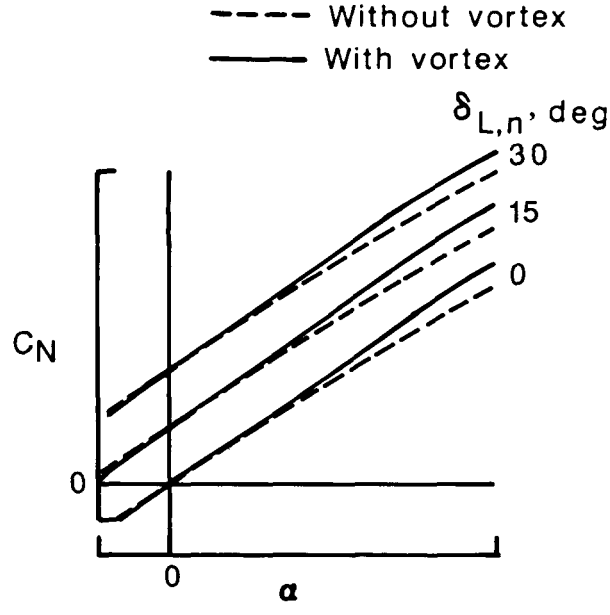

Sketch F

An indication of the value of axial- and normal-force data in the analysis of flap-system performance is given in the following discussion and accompanying sketches. Sketches E and F show the

different nature of the performance benefits of leading- and trailing-edge flaps. The data represent program results obtained by the method described in reference 4 for sharp leading-edge wings. The results shown here include estimates of vortex forces but no leading-edge thrust. Sketch E shows the characteristic near-linear nature of the variation of axial-force coefficient with angle of attack for two leading-edge flap deflections and for the undeflected case. The slope of the "without vortex" line tends to vary linearly with the deflection angle. An envelope of lines representing a series of flap deflections forms a curve approximating the shape of the flat-wing full theoretical leading-edge thrust curve. In effect, a distributed thrust over the flap surface replaces a good portion of the concentrated flat-wing leading-edge thrust. Leading-edge flap deflection also reduces somewhat the wing normal force. The beneficial change in axial force, however, far outweighs this detrimental effect. As described in reference 1, the wing design program of reference 3 and the flap evaluation program of reference 4 can be of help in predicting the required deflection angles for a given lift coefficient. As shown in sketch F, the primary effect of increasing trailing-edge flap deflections is to raise the level of normal-force coefficient throughout the angle-of-attack range. The change in level tends to be proportional to the deflection. There is also a uniform increase in the axial-force coefficient, which tends to increase as the square of the deflection angle. The increased drag resulting from this increased axial force, however, is not as important as the beneficial effect of the increased lift caused by the increased normal force. The performance benefits of trailing-edge flaps are the result of the reduction of angle of attack required for a given lift coefficient. The optimum trailing-edge flap deflection for a given lift coefficient is in turn dependent on the division of load between the trailing-edge flap and the main wing surfaces. The wing-design and analysis programs can be of use in the prediction of this optimum deflection.

In the actual flow about the flap systems, there may be serious departures from the idealized flap behavior discussed in the preceding paragraph. These departures may be greater than those caused by mild leading-edge flow separation, which permits a predominantly attached flow. An example of the use of axial- and normal-force data in assessing the nature of departures from attached flow with vortex separation as calculated by the computer program of reference 4 may be described with the aid of sketches G and H. These data represent a wing-flap system that is operating in a predominantly attached-flow manner for the middle portion of the

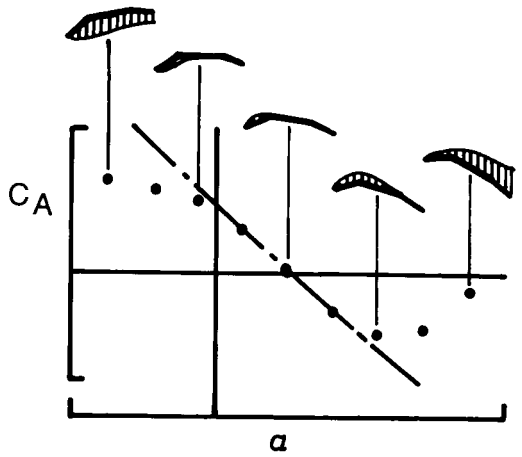

Sketch G

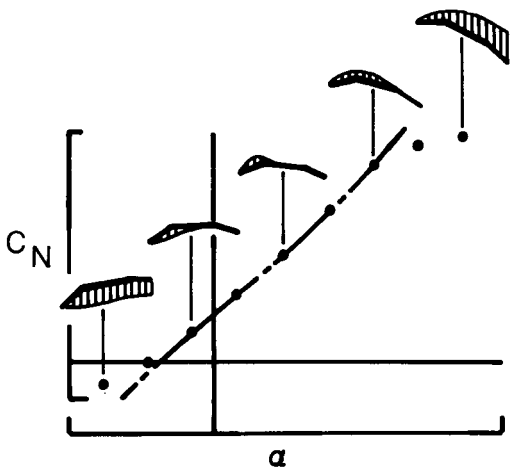

Sketch H

angle-of-attack range shown. However, there is more severe flow separation at higher and lower angles of attack. At an angle of attack large enough to cause the upper-surface separated flow to reattach aft of the leading-edge flap hinge line but ahead of the trailing edge, there is a decrease in distributed thrust on the leading-edge flap surface and an increase in axial force; however, there is little or no loss of normal force. At angles of attack large enough to prevent reattachment ahead of the trailing edge for much of the wing, there is a loss of normal force as well as an increase in axial force. These changes bring about drastic losses in performance. At an angle of attack sufficiently low to cause a lower-surface separation which originates at the wing leading edge but reattaches ahead of the trailing edge, there is a reduction in axial force but little or no change in normal force. For this situation, separated-flow performance may be better than theoretical attached-flow performance. At even lower angles of attack,

the separated flow may not reattach ahead of the trailing edge and the normal force is more positive than for attached flow. In the data analyzed herein, there is only limited evidence of high-angle-of-attack separation (within the range of angles considered), but there is ample evidence of low-angle-of-attack separation.

Computer Program Description

The wing-design program introduced in reference 3 generates an optimized twisted and cambered lifting surface for a given wing planform operating at specified flight conditions, provides the corresponding lifting-pressure distribution, and gives wing force and moment data. The program provides an instantaneous analysis of the designed surface and may be operated in an analysis-only mode. Supersonic as well as subsonic speeds can be handled, but it is not a transonic code. Because the solution is based on the use of candidate surfaces, it can provide a twisted and cambered surface restricted to specified wing regions (a mission-adaptive design) as well as a whole-wing-area design.

The wing-analysis program described in reference 4 is almost identical to the subsonic-analysis portion of the design code described in reference 3. In fact, this program is a predecessor of the design code. For a given camber surface, this program provides lifting-pressure distributions and wing forces and moments. It provides an analysis-only mode and is applicable to subsonic speeds only, but it provides for special handling of flap systems, including simplified flap-geometry input and computed results for various combinations of leading-edge and trailing-edge flap deflections in a single run.

Both programs provide linearized-theory potential-flow solutions for a zero-thickness lifting surface represented by an array of horseshoe vortices and employ a solution by iteration rather than by a matrix inversion. Special integration techniques are employed to account for leading-edge singularities. The programs also provide for an estimate of attainable leading-edge thrust and of the forces caused by separated leading-edge vortices. Attainable leading-edge thrust considerations play a direct part in the design process, but vortex force estimates do not, except for a reduction of design lift coefficient (and camber surface severity) due to the vortex lift contribution. Of course, for the sharp leading edges treated herein, no thrust is realized.

A discussion of the use of the wing-design program, with particular emphasis on leading-edge thrust considerations, is contained in reference 11, and a discussion of the use of both programs for the design and analysis of flap systems with both sharp and rounded leading edges is contained in reference 1.

The computer programs

> WINGDES - Design of Wing Surfaces at Subsonic or Supersonic Speeds, LAR-13315 (see ref. 3)
>
> SUBAERF - Aerodynamic Analysis of Low-Speed Wing Flap Systems, LAR-13116 (see ref. 4)

may be obtained for a fee from:

> COSMIC
> Computer Services Annex
> University of Georgia
> Athens, GA 30602
> (404) 542-3265

Calculations for this paper were made with a version of the "SUBAERF" program, which includes corrections and additions as of April 1985.

Experimental Data

Reference 7 provides a relatively complete set of experimental data for an assessment of the applicability and limitations of the previously described computer programs at low subsonic speeds. The data selected for analysis cover four different planforms and a series of leading- and trailing-edge flap deflections. The wings were constructed of thin materials and, except for the flap deflections obtained by the use of hand-brake equipment, were flat. This geometry provides a valuable simplification in the analysis of some complex aerodynamic phenomena.

The tests were performed in the Northrop 21- by 30-inch low-speed diagnostic facility. Six-component force and moment data were obtained at angles of attack up to and beyond 20° for most configurations. The data were corrected for sting deflection and for blockage and wall effects. Tests were performed at a Mach number of about 0.1 and at Reynolds numbers, based on mean aerodynamic chords, from about 0.35 million to about 0.50 million for the various configurations. As discussed in reference 4, such low Reynolds numbers are generally suspect because of a tendency toward severe flow separation and poor aerodynamic performance. This concern is somewhat alleviated by the very high levels of aerodynamic efficiency that were achieved. There was little evidence of drastic flow separation, except at flap deflections far from optimum settings (wings with no flap deflection at large angles of attack and wings with highly deflected flaps at low angles of attack).

Drawings of the models of reference 7, which provided data used in the present analysis, are shown

in figure 1. The following table lists some of the pertinent model dimensions:

Model	S, in^2	$\bar{c}$, in.	$b/2$, in.	AR
50°-swept cropped delta wing	47.8	5.34	5.08	2.16
60°-swept cropped delta wing	51.1	6.24	4.98	1.94
65°-swept cropped delta wing	59.1	7.49	4.60	1.43
70°/50° cranked leading-edge wing	51.0	7.39	4.59	1.65

The wing reference area S includes the flap areas. Wing and flap geometric data in the form used for input to the computer program of reference 7 are given in table I.

Comparison of Program and Experimental Data

A comparison of results obtained by using the computer program of reference 4 with experimental data scaled from the plots of reference 7 is presented in figures 2 through 6. The wing planform used for the program calculations did not include the fuselage. Sketches of the program planform representation are shown in the figures. For all wings, the lifting surface was represented by an array of elements, each of which had a span one-tenth of the wing semispan and a nominal aspect ratio of 2.0. The number of elements representing the wing planform (both left and right panels) ranged from 380 to 580. As with most numerical methods, the accuracy of the solution is dependent on the degree of discretization. The problem is particularly severe for attached flow on simple hinged flaps. The pressure peaks as shown in sketch B make it difficult to obtain accurate integrated forces with a limited number of elements. The chosen element aspect ratio of 2.0 offers a reasonable compromise between computational costs and the solution accuracy. However, as is shown subsequently, a somewhat better aerodynamic efficiency of the deflected flap systems would have been predicted if a larger number of elements had been employed.

The wing evaluation program has a feature which permits simultaneous solutions for a number of combinations of leading- and trailing-edge flap deflections by use of a perturbation process. This time-saving program option is sufficiently accurate for small deflection angles (streamwise angles of about 20° or less), but because of the large deflection angles treated in this investigation, this feature was not used. For the most part, individual computer runs were performed for each pair of leading- and trailing-edge deflections.

Throughout this paper, the program basic attached-flow solution, which includes no leading-edge thrust forces nor any separated leading-edge vortex forces, is shown by the short-dash line. Program estimated forces for a flow with a separated vortex whose strength is determined by the Polhamus leading-edge suction analogy (ref. 8), and whose location is given by delta-wing empirical data (ref. 4), are shown by the long-dash–short-dash line.

Comparisons of program results and experimental data for the 50°-swept cropped delta wing are presented in figure 2. Figures 2(a) through 2(d) form a series in which the leading-edge flap deflection varies from 0° to 60° measured normal to the hinge line and in which the trailing-edge flap remains undeflected. Figure 2(a) indicates that the flat wing behaves as anticipated. There is little or no leading-edge thrust for the sharp leading-edge wing as shown by the insensitivity of the axial force to angle of attack. As shown by the normal-force curves, the program predicts an appreciable contribution of the vortex force, and the total predicted normal force agrees well with the experimental measurements. The vortex force is apparently responsible for the achievement of a suction parameter S_s of about 0.20 throughout the lift-coefficient range.

Data for the 30° leading-edge flap deflection in figure 2(b) show the characteristic linear variation of axial force with angle of attack for a wing with flap deflection or camber in the leading-edge region. In effect, a distributed leading-edge thrust over the surface of the flap replaces a large part of the theoretical concentrated leading-edge thrust of the flat wing. The reduced value of the theoretical leading-edge thrust caused by the leading-edge flap deflection also reduces the strength of the vortex force according to the Polhamus analogy. There is reasonably good prediction of both axial and normal force over most of the angle-of-attack range. There is also good prediction of drag up to a lift coefficient of about 0.9. This flap deflection produces a maximum suction parameter of about 0.70 at a lift coefficient of about 0.5, which is very close to the program prediction.

For the 45° leading-edge flap deflection of figure 2(c), appreciable discrepancies between theory and experiment begin to appear. However, the differences are not excessively large at an angle of attack of about 16° and a lift coefficient of about 0.8, where this flap deflection produces its maximum lifting efficiency as measured by the suction parameter. The measured suction parameter of this lift coefficient is about 0.68, compared with a value of about 0.52 given by the program results with

vortex effects included. The largest discrepancies between theory and experiment occur at very low lift coefficients, where the measured axial force and drag are much lower than the predicted attached-flow values. This discrepancy occurs because, as discussed previously, a leading-edge flow separation on the undersurface of the highly deflected flap that does not reattach brings about a reduction of the negative normal force on that surface and reduces the axial-force contribution.

With the leading-edge flap deflection increased to 60° in figure 2(d), there are large discrepancies between theory and experiment at all lift coefficients. The only positive feature is a tendency for differences in predicted and measured drag to be smaller in the lift-coefficient range between 0.8 and 1.0, where the best performance is obtained. In other words, as may be observed in most of these correlation figures, the better the actual wing aerodynamic performance the more likely it is that linearized-theory attached-flow methods will be applicable. It is probably not realistic to expect better results from a simple theoretical method for such a large deflection angle. Even the corresponding streamwise deflection angle of about 48° is large. The agreement between predicted and measured moment coefficient must be fortuitous.

Data for the 50° cropped delta wing in figures 2(a), 2(e), and 2(f) may be used to show the effect of trailing-edge flap deflection of up to 30° on the wing performance with undeflected leading-edge flaps. A comparison of these three figures shows that the primary effect of the trailing-edge flaps is to increase the level of wing normal force over the full angle-of-attack range with little change in the slope of the curves. This increase allows a given value of normal force to act on a less-inclined main wing surface which, up to a point of diminishing returns, lowers the drag level. Comparable trailing-edge flap deflections can often match and sometimes exceed the performance benefits of leading-edge flaps. In general, the program results predict quite well the changes in force characteristics due to trailing-edge flap deflection.

Figures 2(g) and 2(h) show data for the 50° cropped delta wing with both leading- and trailing-edge flaps deflected. The 30° leading-edge flap deflection combined with the 15° trailing-edge flap deflection in figure 2(g) gives good performance. A relatively high measured maximum suction parameter of about 0.88 was achieved at a lift coefficient of about 0.7. Program results give a reasonable prediction of this performance. In fact, measured drag is somewhat lower than the program drag throughout the lift-coefficient range. For the larger deflections of figure 2(h), there are large discrepancies between theory and experiment because of the limitations of the linearized-theory method. As is shown subsequently, leading-edge flap deflections of 60° and trailing-edge flap deflections of 30° would be called for only in attempts to optimize performance of this wing at lift coefficients well in excess of 1.0.

Data for the remaining three wings (figs. 3 through 5) cover only the undeflected surface and one or two other specific combinations of leading- and trailing-edge flap deflections. Generally, the same pattern of theoretical-experimental correlation as seen for the 50° cropped delta wing is followed. Reasonably close agreement between predicted and measured results are obtained for the flat surfaces. The vortex provides a substantial contribution to the total normal force. The 30° deflection of the leading-edge flap in combination with the 15° deflection of the trailing-edge flap produces good performance (suction parameters of about 0.80 or more at lift coefficients in the 0.6 to 0.8 range) for each of the wings. In general, the program results agree well with the experimental data for these deflections. At the larger deflection angles ($\delta_{L,n} = 60°$, $\delta_{T,n} = 30°$), there is generally a poor correlation between theory and experiment.

Figure 6 provides data that allow a comparison of the performance of leading-edge flaps of the same area but with different planforms on a 60°-swept leading-edge delta wing. For this comparison, data are available only for leading-edge flap deflections of 30° and trailing-edge flap deflections of 0°. In spite of a noticeable change in flap planform, there is only a small difference in measured force characteristics, and likewise, there is only a small difference in program predictions. The performance of these two flap systems is discussed further in the section "Analysis of Flap Performance."

Analysis of Flap Performance

The purpose of this exercise is to determine as accurately as possible the maximum aerodynamic efficiency of the flap systems and the flap deflections required. This information is helpful in assessing the applicability of linearized-theory attached-flow methods (with or without an account of vortex forces) to the analysis (and presumably the design) of flap systems operating at or near maximum-efficiency conditions.

Figure 7 shows suction parameter as a function of leading-edge flap deflection angle for the three trailing-edge flap deflection angles and for four selected lift coefficients. These suction parameters were found from fairings of experimental data and from the program data curves shown in figures 2 through 5. Each wing planform is treated separately

in figures 7(a) through 7(d). The primary purpose of these plots is to provide data for further analysis. It is worth noting, however, that there is generally a smooth variation of suction parameter with leading-edge flap deflection angle and little evidence of any "peaking" at a specific angle. This indicates that there is not as stringent a requirement for reattachment to occur precisely at the hinge line as might have been supposed from the discussion in the section "Flap Design and Analysis Methodology." Data for a cranked leading-edge wing tested at a Mach number of 0.5 and a Reynolds number of 2.9×10^6 as analyzed in reference 2 displayed sensitivities to leading-edge deflection similar to those shown here, except for a tendency toward more severe penalties for large deflections, that are possibly associated with hinge-line separation.

The data shown in figures 8(a) through 8(d) have been obtained from the plots of the corresponding parts of figure 7. For each of the selected lift coefficients, the restricted maximum suction parameter $S_{s,\max,L}$ and the corresponding optimum leading-edge flap deflection $\delta_{L,n,\text{opt}}$ from figure 7 are plotted as functions of trailing-edge flap deflection. These plots are then used to determine an unrestricted maximum suction parameter $S_{s,\max}$, the corresponding optimum trailing-edge flap deflection angle $\delta_{T,n,\text{opt}}$, and the accompanying optimum leading-edge flap deflection angle $\delta_{L,n,\text{opt}}$. At the bottom of each part of figure 8, the final or unrestricted maximum suction parameter and the corresponding optimum leading- and trailing-edge flap deflection angles are shown as functions of lift coefficient. As expected, the optimum suction parameter is relatively constant over the lift-coefficient range, and both the optimum leading-edge deflection and the optimum trailing-edge deflection tend to vary linearly with lift coefficient. For the most part, there is good agreement between measured and predicted optimum deflections and only a small tendency for the program to underestimate the performance level. It is shown subsequently that a part of this underprediction is caused by the inability of numerical methods to fully account for the effects of attached-flow hinge-line singularities. As shown by the difference between the "with-vortex" and the "without-vortex" program curves, the vortex contribution at optimum conditions is appreciable only at the larger lift coefficients. These results support the applicability of linearized-theory attached-flow methods (with approximate representation of vortex forces) to the analysis (and presumably the design) of efficient flap systems. In effect, for near-optimum flap settings, the attached-flow solution models the major portion of the forces generated by the actual separated flow, even though the attached and separated flow fields have an entirely different structure. Even attached-flow methods that do not take vortex forces into account can be used for the selection of optimized flap-system geometry, but design-point performance levels at high Reynolds numbers tend to be underestimated unless vortex forces are included.

The data of figures 7 and 8 show clearly that both leading-edge and trailing-edge flaps are required for performance maximization. The data also show that near-maximum performance can be achieved over a fairly broad range of leading- and trailing-edge flap deflection angles on either side of the indicated optimum angles.

In figure 8(d), there is a notable overestimation of the optimum leading-edge flap deflection for the lift coefficients approaching 1.0. There is also a tendency toward the underestimation of the required trailing-edge flap deflection. This phenomenon was also encountered in the study of reference 2. Data analyzed in that report showed an abrupt loss of lifting efficiency at $C_L = 0.8$ as leading-edge flap deflections were increased beyond the theoretical optimum for a $70°/20°$ cranked leading-edge wing tested at a Mach number of 0.5 and a Reynolds number of 2.9 million. It is perhaps significant that similar penalties of leading-edge flap deflection beyond theoretical optimums were observed in the present analysis only for the $70°/50°$ cranked leading-edge wing. There is much yet to be learned about the influence of Mach number and Reynolds number on flap-system performance.

Another way of examining flap-system aerodynamic performance is through the use of contour maps such as those shown in figure 9. This figure provides only a sample of the use of performance maps. Data are shown for the four wings, but only for a lift coefficient of 0.8. The contour lines of constant suction parameter give an indication of the performance given by various combinations of leading- and trailing-edge deflections and serve to identify maximum performance and optimum deflections. An advantage of such plots is that other aerodynamic characteristics that influence the selection of deflection angles may be superimposed. For the examples shown herein, contour lines of pitching-moment coefficient have been added. As with the data of figure 8, there is reasonable agreement between the program theoretical and experimental optimum angles, and there is a tendency of the theory to underpredict the maximum suction parameter. In general, there is also a reasonable agreement between pitching-moment contours, so that if it became necessary to limit the pitching moment (e.g., to minimize trim drag), the program results would serve as a good

guide in the absence of experimental data. For example, if it were necessary to restrict the pitching moment to values no less than 0.04 at $C_L = 0.8$ for the 50° cropped delta wing, experimental data would give the best performance at about $\delta_{L,n} = 38°$ and $\delta_{T,n} = 5°$, and program data would give the best performance at about $\delta_{L,n} = 34°$ and $\delta_{T,n} = 5°$.

Data for the 60° cropped delta wing with different leading-edge flap planforms are presented in figure 6. Figure 10 provides a closer examination of performance differences. Unfortunately, this comparison can be made for only one leading-edge flap deflection, and no comparison data with trailing-edge flap deflections are available. For the 30° leading-edge flap deflection, the experimental data show a small advantage for the tapered flap over the vortex design. Program data also show better performance for the tapered flap, but by a smaller margin. However, in data not shown herein, the program predicted essentially the same performance for the two flap planforms when both leading- and trailing-edge flaps are employed and when deflections are optimized.

As mentioned previously, the accuracy of the program attached-flow solution depends on the detail of the lifting-surface representation. A problem can arise because of the theoretical hinge-line singularities in the pressure distribution and the difficulty of accurately representing these singularities in the numerical integration process. With the present method, the only way of approaching a true theoretical solution is by reducing the size and increasing the number of wing elements. As part of this study, an estimate of numerical errors caused by practical limits on element size has been made. For this exercise, the element aspect ratio serves as the variable that dictates element size and number. Changes in element aspect ratio are more effective than changes in element span in obtaining better representation of hinge-line singularities. An example of the variation of the program suction parameter with element aspect ratio is given in sketch I. These data are for the 50° cropped delta wing with $\delta_{L,n} = 30°$, $\delta_{T,n} = 15°$, and $C_L = 0.8$. The scale has been chosen to permit inclusion of an infinite element aspect ratio. The scale is linear in the reciprocal of the aspect ratio. For this representative example, the extrapolated suction parameter for an infinite aspect ratio is greater than that for the nominal aspect ratio of 2.0, used throughout the paper, by about 0.06. For $\delta_{L,n} = 60°$ and $\delta_{T,n} = 30°$, the difference is somewhat smaller, and for undeflected flaps there is essentially no difference. Additional examples of the difference between suction parameters given by the nominal element aspect ratio of 2.0 and by the extrapolation are given in figure 11. These data repeat the plots of maximum suction parameter versus lift coefficient shown in figure 8, except that the program data are estimated for an extrapolation to an element aspect ratio of infinity. Generally, the extrapolation to a presumably more accurate attached-flow solution improves the theoretical-experimental correlation. However, in view of the complications involved and the reasonable results obtained without extrapolation, such a procedure is rarely required. It was done in this instance only to show the closer agreement with experiment that could be obtained with a more exact attached-flow solution.

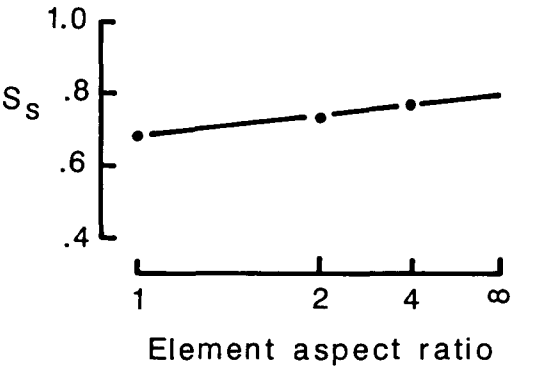

Sketch I

Study of Flap Design Concept

The flap-system design approach discussed in references 1 and 2, of course, was not used in the selection of the flap systems tested in reference 7 and analyzed in the preceding section of this paper. However, in view of the good performance of the tested flap systems, it would be instructive to apply the design process to these wing planforms and compare the resultant flap surfaces with those found to offer good performance. The 60° cropped delta wing is used for an example because for that wing, data (although limited) are available for two leading-edge flap planforms. Figure 12 shows a camber surface generated by the wing-design program of reference 4 for the 60° cropped delta wing at a selected design lift coefficient $C_{L,\text{des}}$ of 0.7. This, according to the terminology of reference 1, is a "whole-wing" design. There is, however, one significant difference between this example and those of reference 1. For this design, the program default set of chords for leading-edge modification surface was replaced by an input set of chords corresponding to the actual wing planform chords. This change yielded a wing surface with less spanwise twist, which made an easier task of fitting flap surfaces to the design camber surface. There was also a small increase in the suction parameter.

As stated in reference 3, program defaults provide candidate surfaces which generally provide a camber surface design with good aerodynamic efficiency, but it is suggested that the program user may want to tailor a camber-surface solution more appropriate to the problem at hand and may want to search for solutions offering greater efficiency.

Figure 12 shows the wing design program lifting-surface ordinates nondimensionalized with respect to the wing root chord as a function of distance behind the leading edge nondimensionalized with respect to the wing root chord. Airfoil section mean-camber surfaces are shown for 10 semispan locations from $\frac{y}{b/2} = 0.05$ to $\frac{y}{b/2} = 0.95$. For convenience, the program-generated wing camber surface is shown for a reference angle of attack of 0°. An appreciable spanwise twist results from the spanwise growth in upwash at the leading edge for this swept leading-edge wing. The wing-design process utilizes this upwash to generate lift on surfaces which are inclined so as to produce a distributed-thrust force. According to program estimates, this camber surface should provide a relatively high aerodynamic efficiency, a suction parameter of 0.95 at the design conditions. A well-designed flap system should attempt to match as closely as possible the surface and, thus, the loadings of the camber-surface design. Particular attention should be paid to the wing outboard stations, where most of the distributed thrust is developed. The solid line represents an attempt to approximate the design camber surface through a schedule of deflections of the leading- and trailing-edge flap segments as shown in the plots on the right-hand side of the figure. To approximate the outboard section ordinates, it was necessary to rotate the flat-wing surface to a reference angle of attack of −10°. There was no need to alter the original leading-edge flap chord schedule to fit the flap surface to the camber surface. A much better fit could have been made if it were possible to increase the chord of the trailing-edge flap at the inboard span stations. For this design, however, the original trailing-edge flap chord was retained, and the flap deflection was selected to match the slope of the camber surface at the wing trailing edge. This should tend to preserve the design section normal force.

In figure 12, the plot of the fitted leading-edge flap deflections shows that a single-segment leading-edge flap would require an optimum streamwise deflection of just under 20°. This agrees well with the experimentally determined optimum for the design conditions, which was about 32° measured normal to the hinge line or about 17° measured in the streamwise direction. The fitted trailing-edge flap deflection of about 15° also corresponds reasonably well with the experimental optimum of about 18°. The requirement for a larger deflection than that given by the design method should be expected, because the actual trailing-edge flap does not extend to the wing centerline.

As noted previously, for the 60° cropped delta wing, the tapered leading-edge flap with the larger inboard chord performed better than the vortex design. This comparison, however, was made only for the case of undeflected trailing-edge flaps; it should be interesting to apply the wing design program to this situation. Because the trailing-edge flap has a dominant effect on the wing pitching moment, the design program was used to generate an optimum lifting surface for this wing at $C_{L,\text{des}} = 0.7$ with an imposed pitching-moment coefficient restraint of 0.05, which is the experimental pitching-moment coefficient generated by the wing with no trailing-edge flap deflection. This should call for a design surface with only small slopes in the trailing-edge region. The results of the computer program design process are shown in figure 13. As before, a flap system was chosen to match as closely as possible the surface given by the design program. Particular attention was given to the outboard span stations. The resultant leading-edge flap deflection schedule is shown in the plot on the right-hand side of figure 13. There is a subtle difference between this design surface and that for the unrestricted pitching moment shown in figure 12. Here, there is a larger curvature in the inboard leading-edge region of the wing, such that a better surface match is provided by the larger inboard chords of the tapered flap. Thus, there is at least a qualitative agreement between the observed phenomenon and the results of the predominantly attached-flow numerical methods.

The discontinuous sweep of the 70°/50° cranked leading-edge wing presents a problem in the selection of optimum leading-edge flap deflection angles. Test results were gathered for flap deflections measured normal to the hinge line that were the same for both inboard and outboard wing panels. It is possible, however, that better performance could be obtained with another arrangement. A wing-design program example (fig. 14) was used to study the problem. For this purpose, the mission-adaptive design feature of the program was applied for a design lift coefficient of 0.7 and for an unrestricted moment coefficient. The sketch at the top of figure 14 delineates the wing areas affected by the mission-adaptive design. Design area chords are taken to be about one and one-half times the actual flap chords. As illustrated in figure 14, this provides a convenient way of defining flap surface slopes by extending the midregion surface to the flap hinge-line location and connecting this point to either the wing leading or trailing edge as

appropriate. In using the program for this purpose, it is neither necessary nor desirable to use more trailing-edge candidate surfaces than trailing-edge flap segments. For this example, the single-segment trailing-edge flap requires only the first trailing-edge candidate surface, which results in a constant deflection angle.

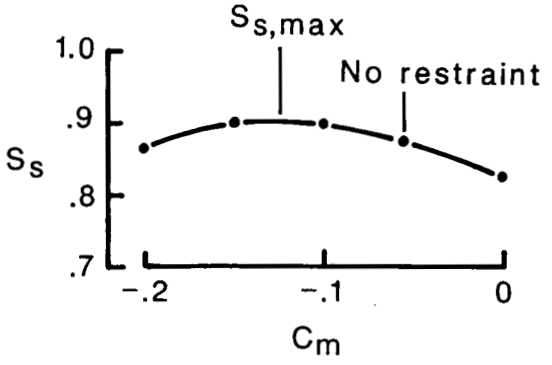

Sketch J

For this design problem, no restraint was placed on pitching moment. Application of the mission-adaptive design option to problems of this sort has shown that the numerical solutions tend to call for greater use of leading-edge surfaces and less use of trailing-edge surfaces than would a true optimum design. The difficulty seems to be associated with a design process that uses normal and axial forces instead of lift and drag in the optimization procedures. This characteristic is common to all linearized-theory design methods because of a fundamental assumption that all surface slopes are small. The problem does not arise to any appreciable extent for the whole-wing design, but does affect results for the mission-adaptive design where relatively large surface slopes are needed to generate the required loadings on restricted areas. An improved design can be found by running the mission-adaptive design program for a selected series of design pitching-moment coefficients and using a plot such as that shown in sketch J. The unrestrained design provides a suction parameter of about 0.88 and a $C_{m,\text{des}}$ value of about −0.06, whereas an optimum suction parameter of about 0.90 occurs for a $C_{m,\text{des}}$ value of −0.12. This large negative moment might present a trim drag problem in an airplane design project. When horizontal-tail contributions or canard trim contributions are considered in the definition of a desired wing moment coefficient, and when that moment is specified as a wing-design program input, a better overall design should result. In that case, the previously described search for optimum performance of the wing alone is avoided.

The dashed line on the typical airfoil section of figure 14 shows the design surface for the $C_{m,\text{des}} = -0.12$ restraint, and the solid line shows the selected flap deflection for that section. The plots at the bottom of figure 14 show the spanwise distribution of leading- and trailing-edge flap deflections that are dictated by the design program results. For comparison, the dashed line in these plots shows the deflection angles that the experimental data showed to be optimum. The experimental-optimum uniform hinge-line deflection of about 35° translates to streamwise angles of 11.5° and 27.2° for the inboard and outboard panels. The design program data, however, indicate that the schedule of the streamwise deflection angle should be much more uniform. Although the experimental-optimum leading-edge flap deflection is smaller than the theoretical-optimum deflection, the experimental-optimum trailing-edge flap deflection is larger. As pointed out in references 1 and 2 and previously in this paper, this difference is probably the result of flow separation not restricted to the leading-edge flap surface.

Conclusions

An analysis of the low-speed aerodynamic performance of simple hinged flap systems for thin swept wings with sharp leading edges has led to the following conclusions:

1. Linearized-theory attached-flow computer program methods (with approximate representation of vortex forces) can form the basis of a rational flap design and analysis system.
2. Even attached-flow methods that do not take vortex forces into account can be used for the selection of optimized flap-system geometry, but design-point performance levels at high Reynolds numbers tend to be underestimated unless vortex forces are included.
3. Both leading- and trailing-edge flaps are needed for maximum performance, and the required deflection angles can be predicted with reasonable accuracy. Also, near-maximum performance can be achieved over a fairly broad range of deflection-angle combinations.
4. For design problems in which pitching-moment restraints must be imposed, program estimates can be used to predict the necessary limitations on flap deflections and the resultant change in lifting efficiency.
5. Sample applications of the wing-design program showed reasonable agreement between optimized wing surfaces and the surfaces formed by flap systems operating at optimum deflections.

The important influence of Mach number and Reynolds number on flap-system performance was not addressed in this study, nor were the effects of rounded leading edges considered. The conclusions are restricted to thin swept wings with sharp leading edges at low subsonic Mach numbers and at Reynolds numbers sufficiently high to avoid appreciable performance degradation at or near design conditions.

NASA Langley Research Center
Hampton, VA 23665-5225
November 17, 1986

References

1. Carlson, Harry W.: *The Design and Analysis of Simple Low Speed Flap Systems With the Aid of Linearized Theory Computer Programs.* NASA CR-3913, 1985.
2. Carlson, Harry W.; and Darden, Christine M.: *Attached Flow Numerical Methods for the Aerodynamic Design and Analysis of Vortex Flaps. Vortex Flow Aerodynamics, Volume II,* James F. Campbell, Russell F. Osborn, and Jerome T. Foughner, Jr., eds., NASA CP-2417, 1986, pp. 111-122.
3. Carlson, Harry W.; and Walkley, Kenneth B.: *Numerical Methods and a Computer Program for Subsonic and Supersonic Aerodynamic Design and Analysis of Wings With Attainable Thrust Considerations.* NASA CR-3808, 1984.
4. Carlson, Harry W.; and Walkley, Kenneth B.: *An Aerodynamic Analysis Computer Program and Design Notes for Low Speed Wing Flap Systems.* NASA CR-3675, 1983.
5. Lamar, John E.: Subsonic Vortex-Flow Design Study for Slender Wings. *J. Aircr.,* vol. 15, no. 9, Sept. 1978, pp. 611–617.
6. Lamar, John E.; Schemensky, Roy T.; and Reddy, C. Subba: Development of a Vortex-Lift Design Procedure and Application to a Slender Maneuver-Wing Configuration. *J. Aircr.,* vol. 18, no. 4, Apr. 1981, pp. 259–266. (Available as AIAA-80-0327R.)
7. Carey, K. M.; and Erickson, G. E.: *Vortex Flap Technology: A Stability and Control Assessment.* NASA CR-172439, 1984.
8. Polhamus, Edward C.: Predictions of Vortex-Lift Characteristics by a Leading-Edge Suction Analogy. *J. Aircr.,* vol. 8, no. 4, Apr. 1971, pp. 193–199.
9. Rao, Dhanvada M.: Leading-Edge 'Vortex Flaps' for Enhanced Subsonic Aerodynamics of Slender Wings. *ICAS Proceedings 1980—12th Congress of the International Council of the Aeronautical Sciences (ICAS),* J. Singer and R. Staufenbiel, eds., 1980, pp. 554–562. (Available as ICAS-80-13.5.)
10. Frink, Neal T.: Critical Evaluation of a Vortex Flap Design Concept Using a 74° Delta Configuration. *Vortex Flow Aerodynamics, Volume II,* James F. Campbell, Russell F. Osborn, and Jerome T. Foughner, Jr., eds., NASA CP-2417, 1986, pp. 17–37.
11. Carlson, Harry W.; Shrout, Barrett L.; and Darden, Christine M.: Wing Design With Attainable Leading-Edge Thrust Considerations. *J. Aircr.,* vol. 22, no. 3, Mar. 1985, pp. 244–248.

Table I. Wing Planform Input Data for the Computer Program of Reference 7

50°-swept cropped delta wing

```
SREF=47.8,CBAR=5.34,XMC=4.22,
NLEY=5,TBLEY=0.0,0.64,1.12,4.50,5.08,
       TBLEX=0.0,0.51,0.90,4.97,5.83,
NTEY=2,TBTEY=0.0,5.08,
       TBTEX=7.42,7.42,
NLEFY=6,TBLEFY=0.0,0.63,0.64,1.12,4.50,5.08,
        TBLEFC=0.0,0.00,0.46,0.61,0.61,0.42,
NTEFY=6,TBTEFY=0.0,0.63,0.64,4.20,4.21,5.08,
        TBTEFC=0.0,0.00,0.94,0.48,0.00,0.00,
```

60°-swept cropped delta wing

```
SREF=51.1,CBAR=6.24,XMC=5.36,
NLEY=4,TBLEY=0.0,0.64,4.56,4.98,
       TBLEX=0.0,0.69,7.38,8.34,
NTEY=2,TBTEY=0.0,4.98,
       TBTEX=9.11,9.11
NLEFY=5,TBLEFY=0.0,0.63,0.64,4.56,4.98,
        TBLEFC=0.0,0.0,0.66,1.06,0.80,
NTEFY=6,TBTEFY=0.0,0.63,0.64,4.17,4.18,4.98,
        TBTEFC=0.0,0.00,1.16,0.38,0.00,0.00,
```

65°-swept cropped delta wing

```
SREF=59.1,CBAR=7.49,XMC=5.67,
NLEY=5,TBLEY=0.0,0.64,1.26,4.17,4.60,
       TBLEX=0.0,0.64,1.26,7.19,8.22,
NTEY=2,TBTEY=0.000,4.600,
       TBTEX=10.17,10.17,
NLEFY=6,TBLEFY=0.0,0.63,0.64,1.26,4.17,4.60,
        TBLEFC=0.0,0.00,0.33,1.03,1.40,1.22,
NTEFY=6,TBTEFY=0.0,0.63,0.64,3.81,3.82,4.60,
        TBTEFC=0.0,0.00,1.34,0.61,0.00,0.00,
```

70°/50° cranked leading-edge wing

```
SREF=51.0,CBAR=7.39,XMC=5.82,
NLEY=4,TBLEY=0.0,0.64,3.17,4.59,
       TBLEX=0.0,0.46,7.44,9.14,
NTEY=2,TBTEY=0.000,4.590,
       TBTEX=10.26,10.26,
NLEFY=6,TBLEFY=0.0,0.63,0.64,2.50,3.17,4.59,
        TBLEFY=0.0,0.00,0.90,1.96,0.82,0.37,
NTEFY=6,TBTEFY=0.0,0.63,0.64,3.77,3.78,4.59,
        TBTEFC=0.0,0.00,1.35,0.50,0.00,0.00,
```

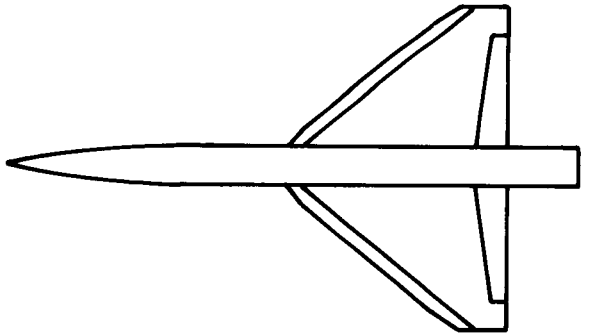

50°-swept cropped delta wing

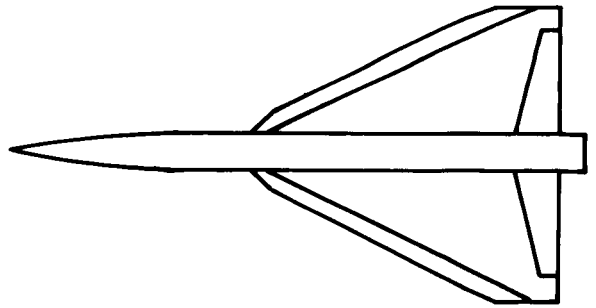

65°-swept cropped delta wing

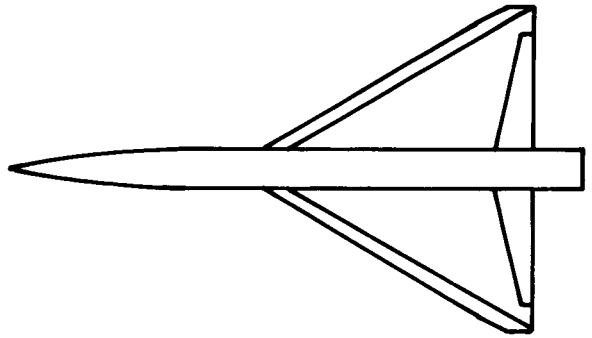

60°-swept cropped delta wing

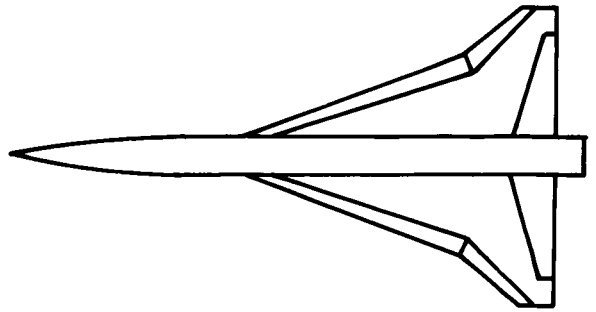

70°/50° cranked leading-edge wing

Figure 1. Drawings of selected models tested in reference 7 and used for this study.

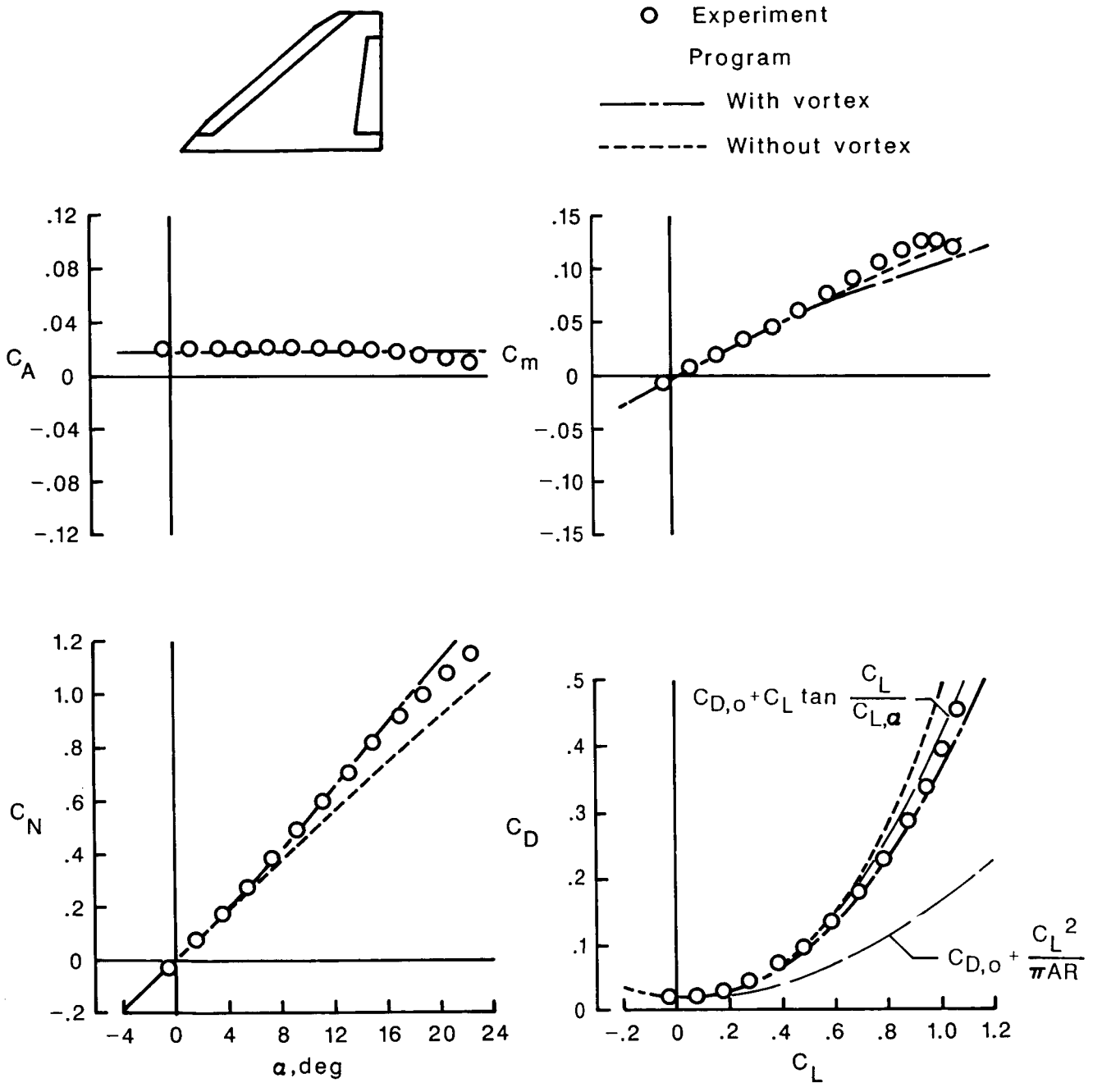

(a) $\delta_{L,n} = 0°$, $\delta_{T,n} = 0°$.

Figure 2. Comparison of program results and experimental data for 50°-swept cropped delta wing.

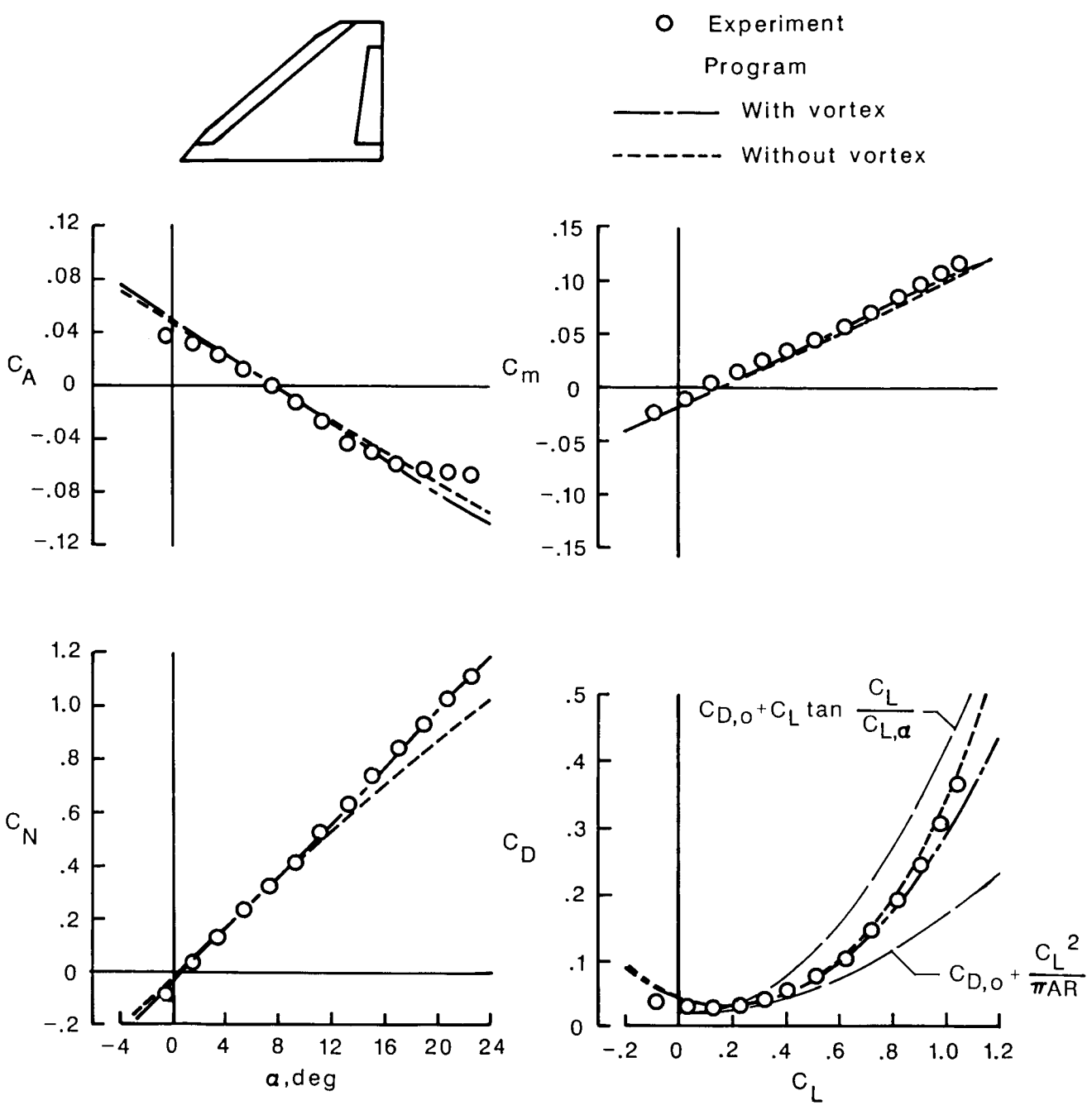

(b) $\delta_{L,n} = 30°$, $\delta_{T,n} = 0°$.

Figure 2. Continued.

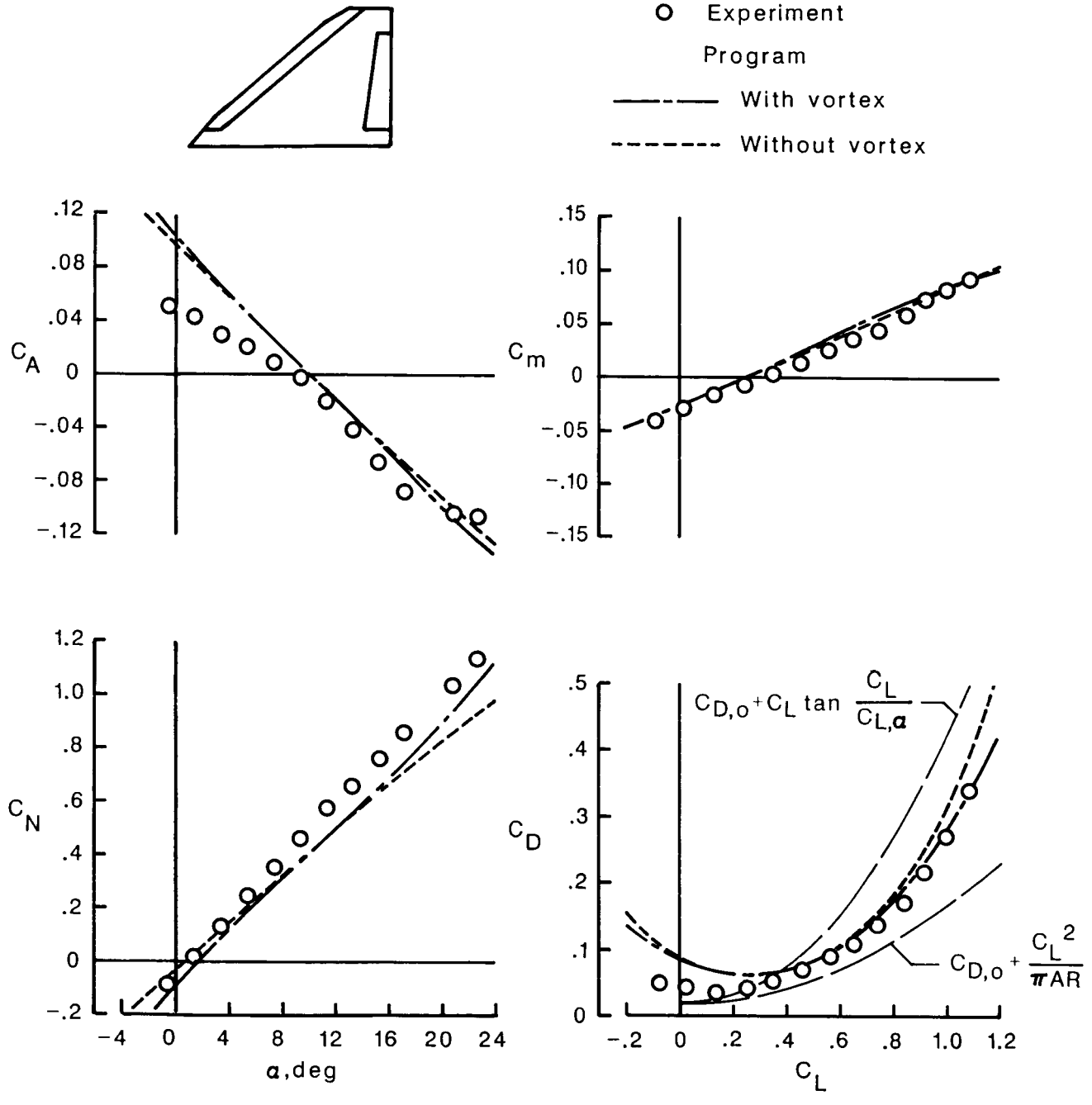

(c) $\delta_{L,n} = 45°$, $\delta_{T,n} = 0°$.

Figure 2. Continued.

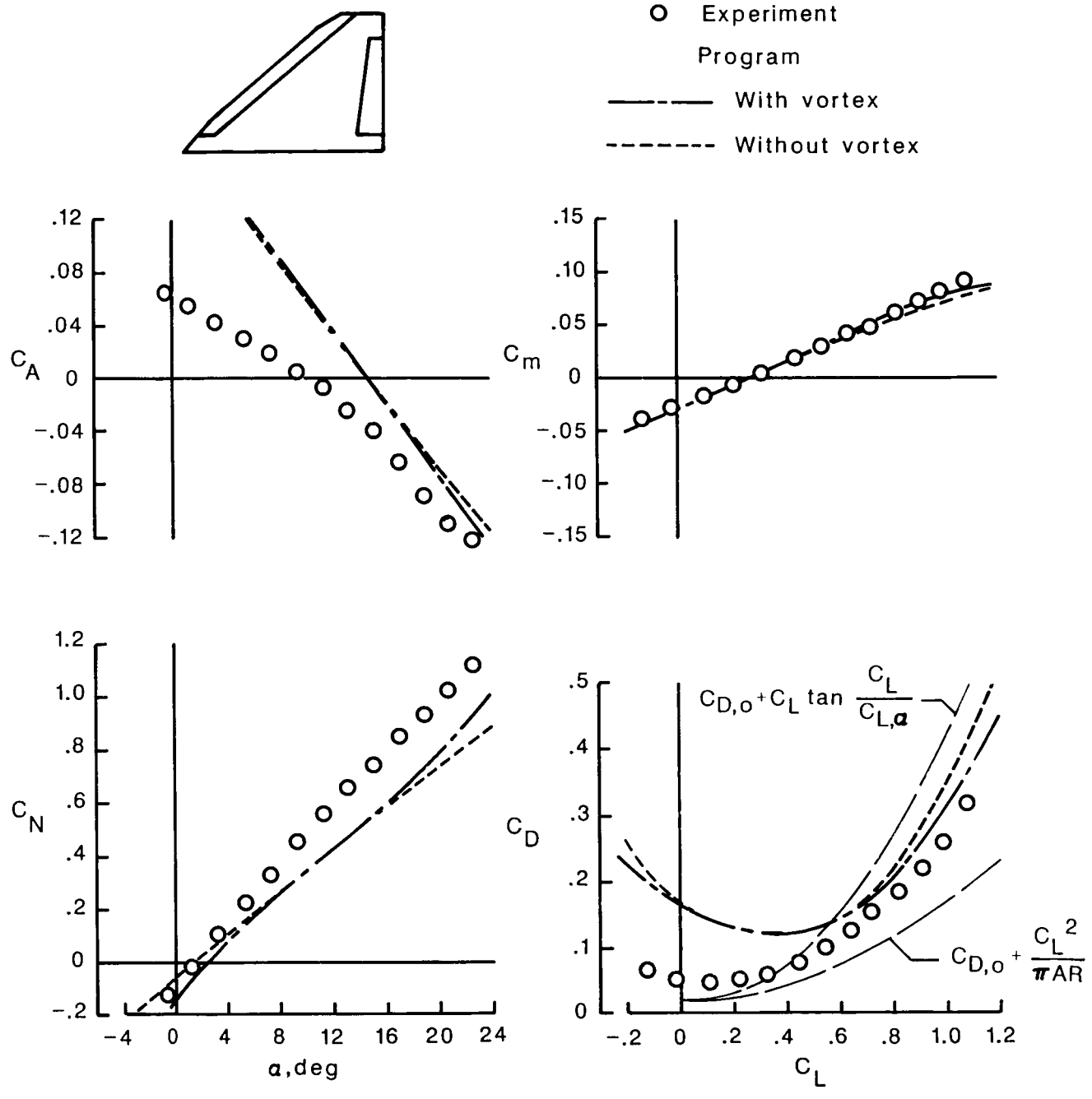

(d) $\delta_{L,n} = 60°$, $\delta_{T,n} = 0°$.

Figure 2. Continued.

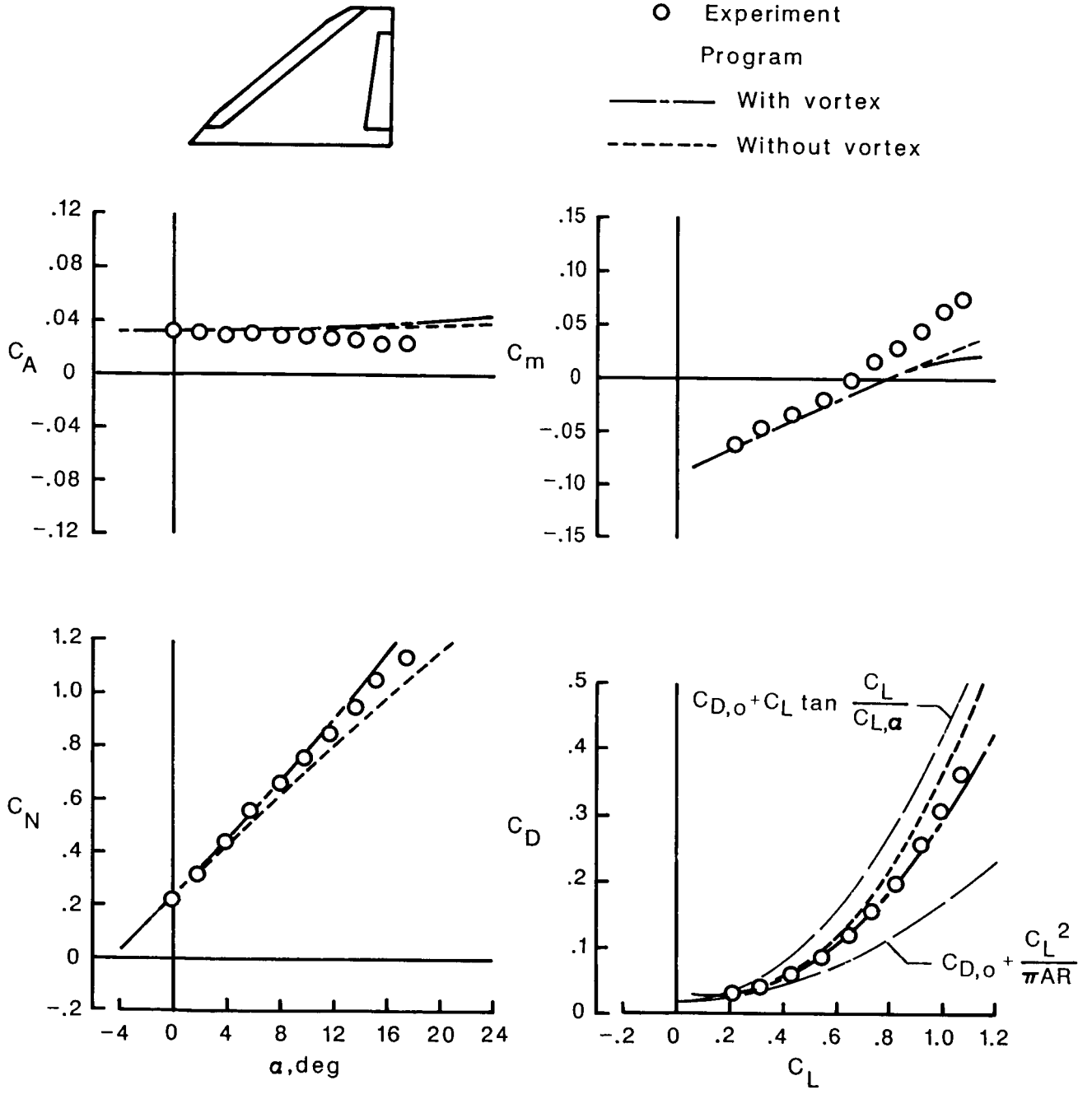

(e) $\delta_{L,n} = 0°$, $\delta_{T,n} = 15°$.

Figure 2. Continued.

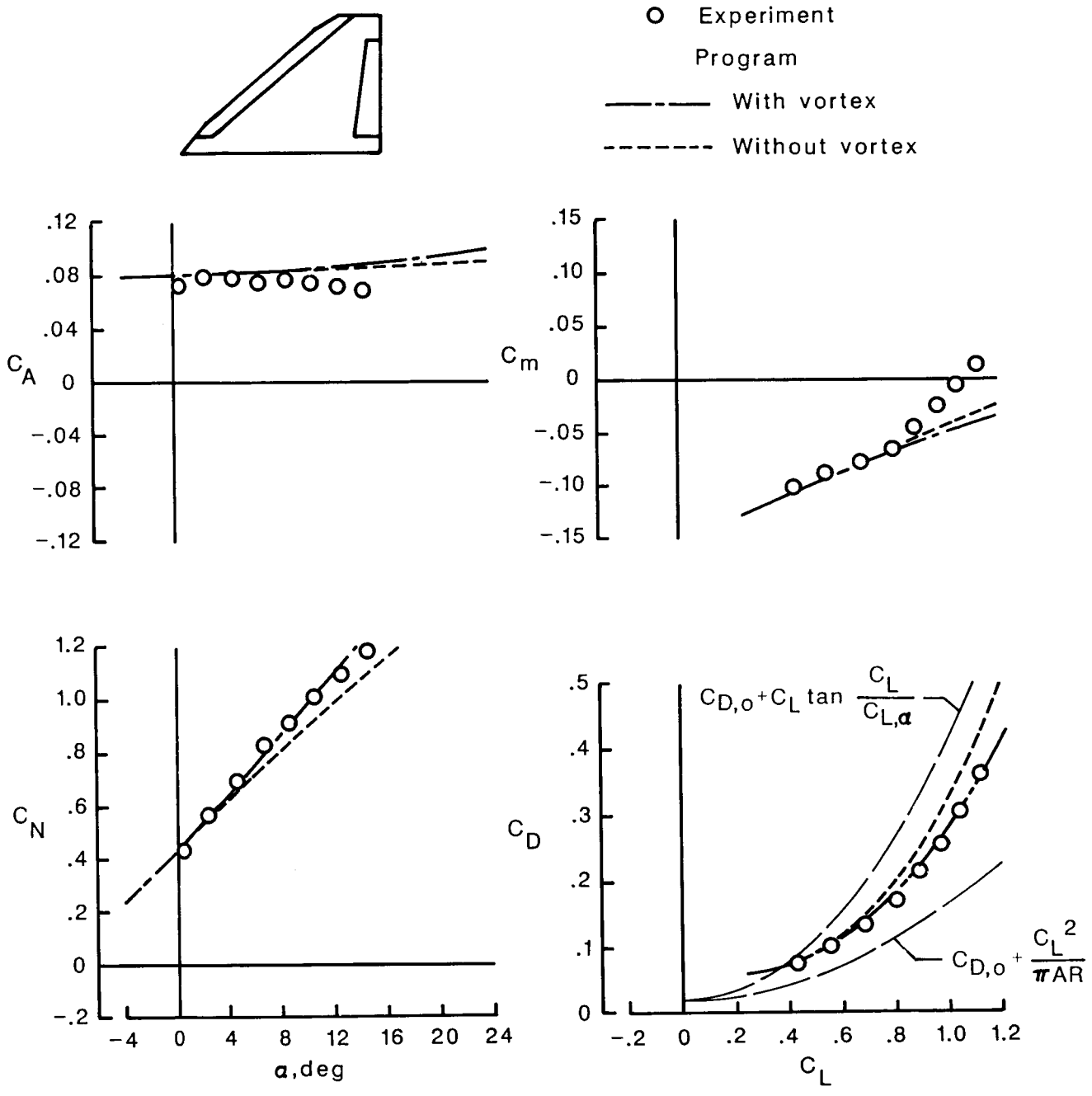

(f) $\delta_{L,n} = 0°$, $\delta_{T,n} = 30°$.

Figure 2. Continued.

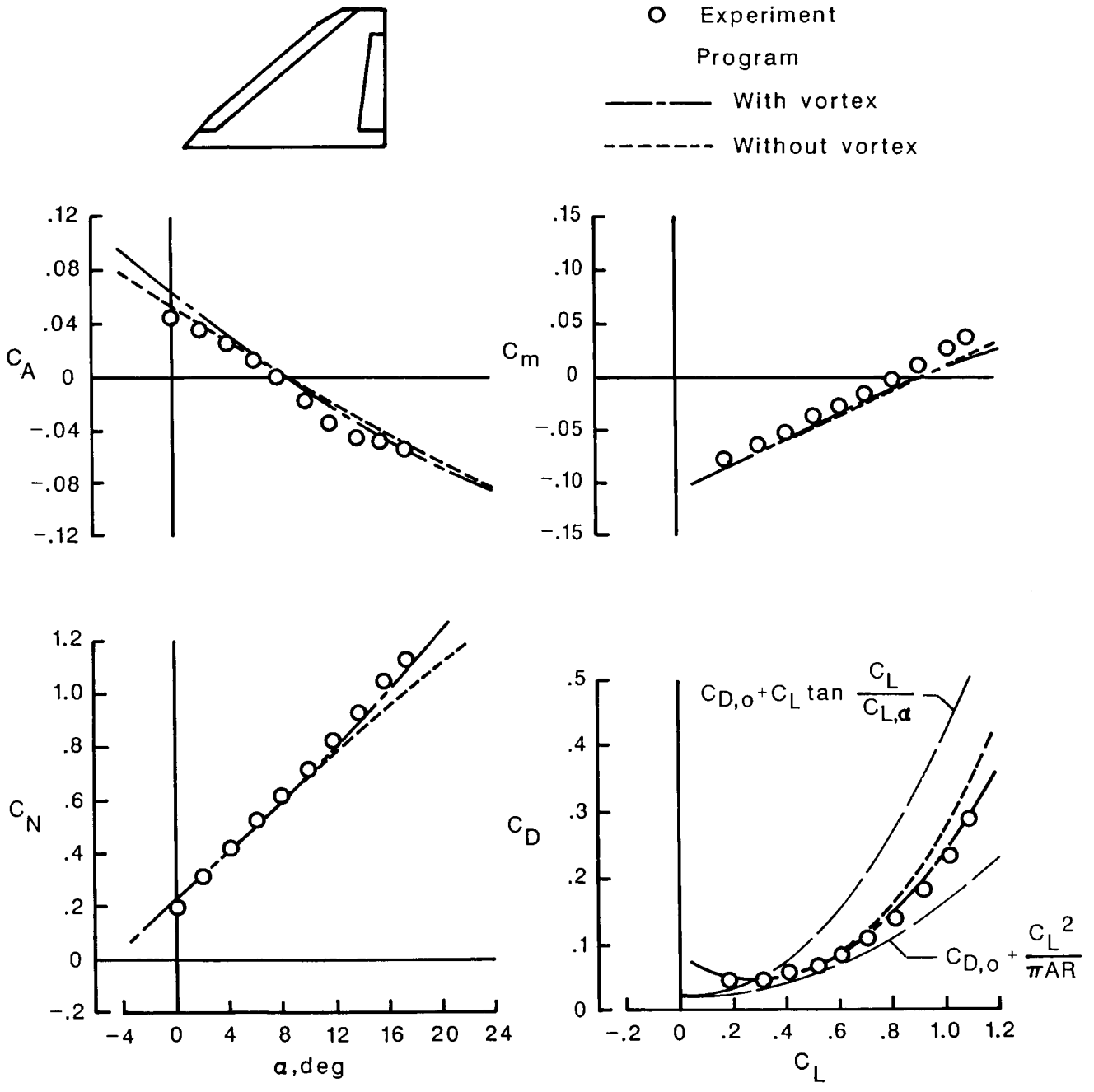

(g) $\delta_{L,n} = 30°$, $\delta_{T,n} = 15°$.

Figure 2. Continued.

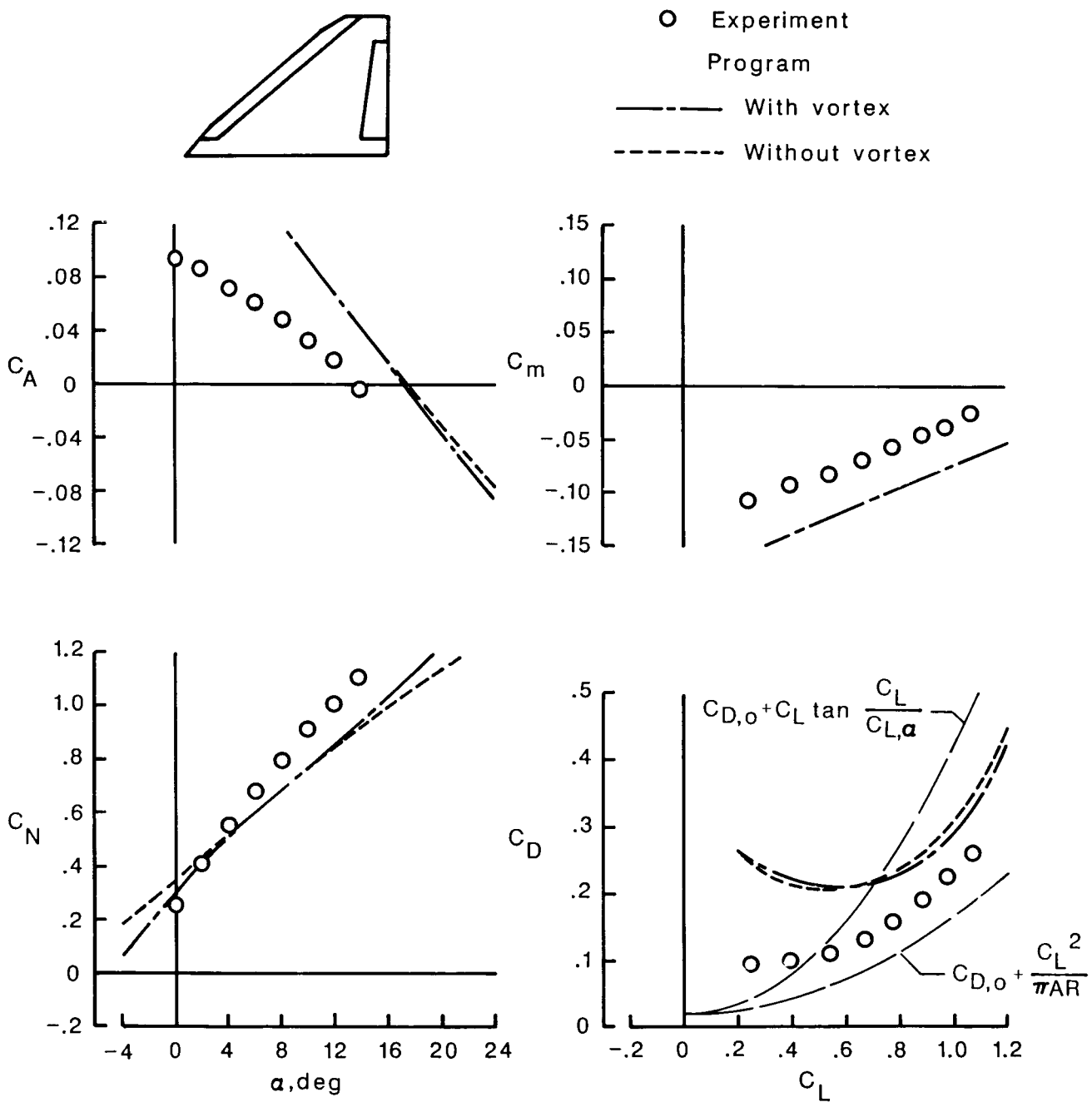

(h) $\delta_{L,n} = 60°$, $\delta_{T,n} = 30°$.

Figure 2. Concluded.

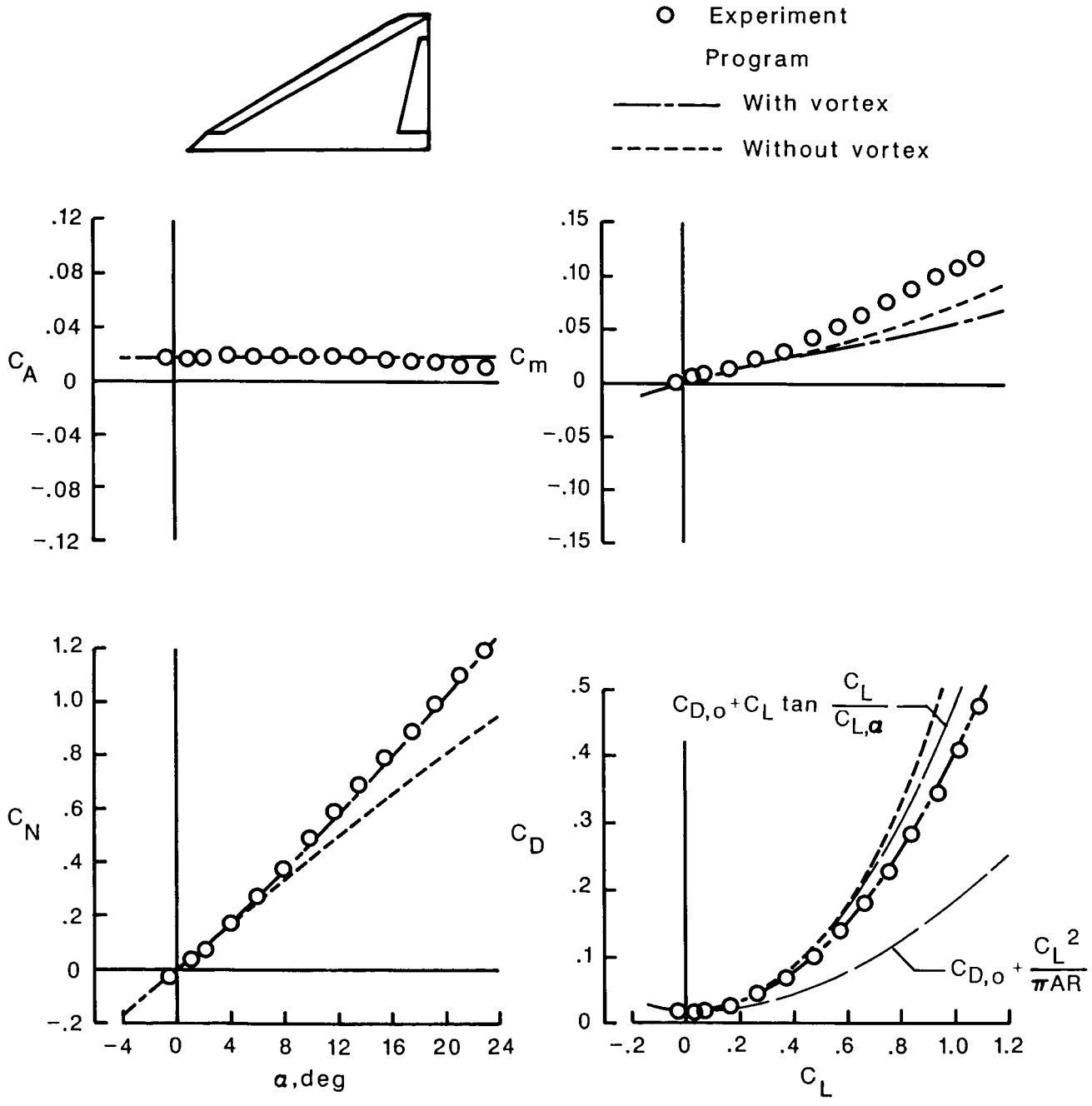

(a) $\delta_{L,n} = 0°$, $\delta_{T,n} = 0°$.

Figure 3. Comparison of program results and experimental data for 60°-swept cropped delta wing.

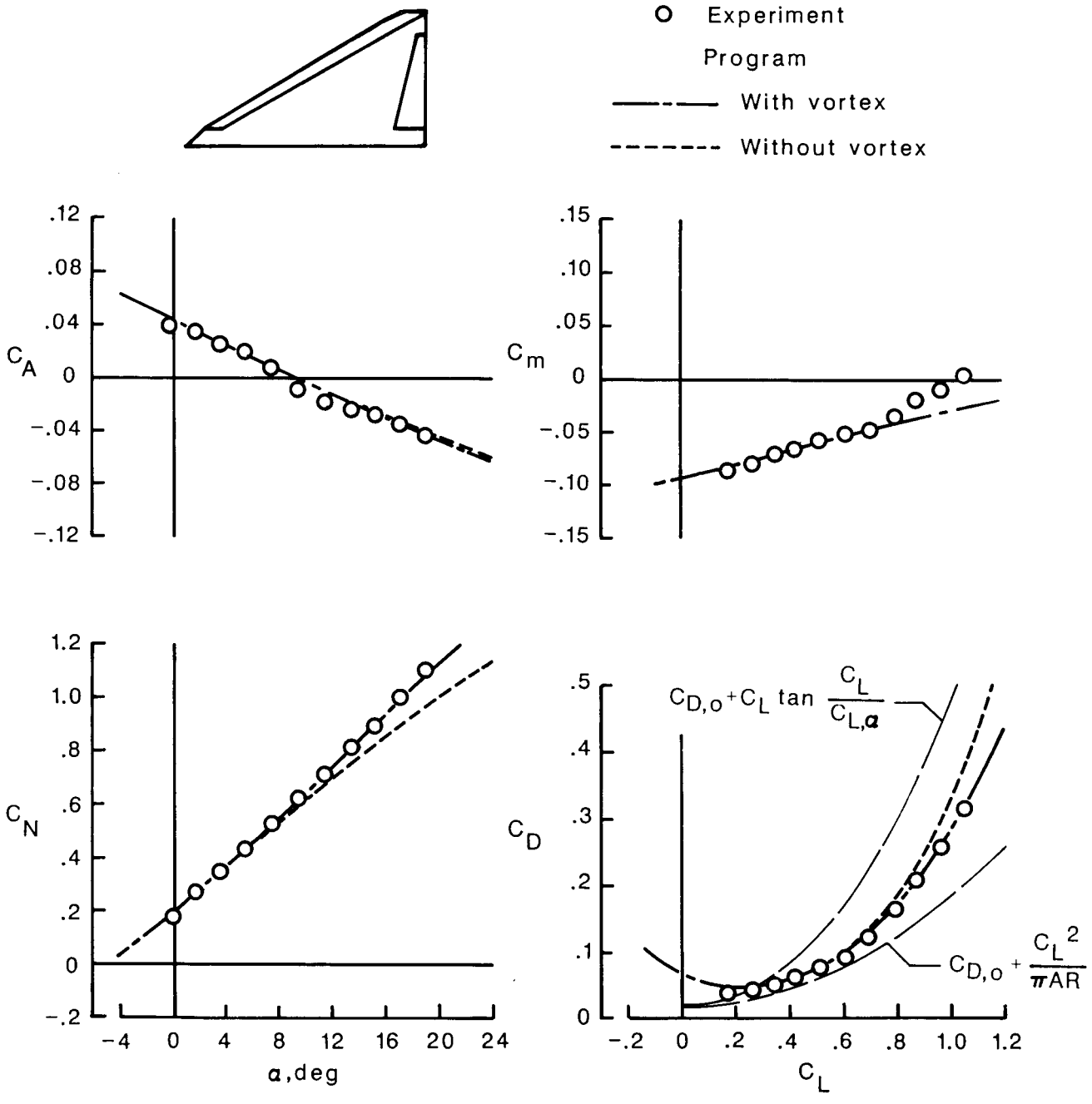

(b) $\delta_{L,n} = 30°$, $\delta_{T,n} = 15°$.

Figure 3. Continued.

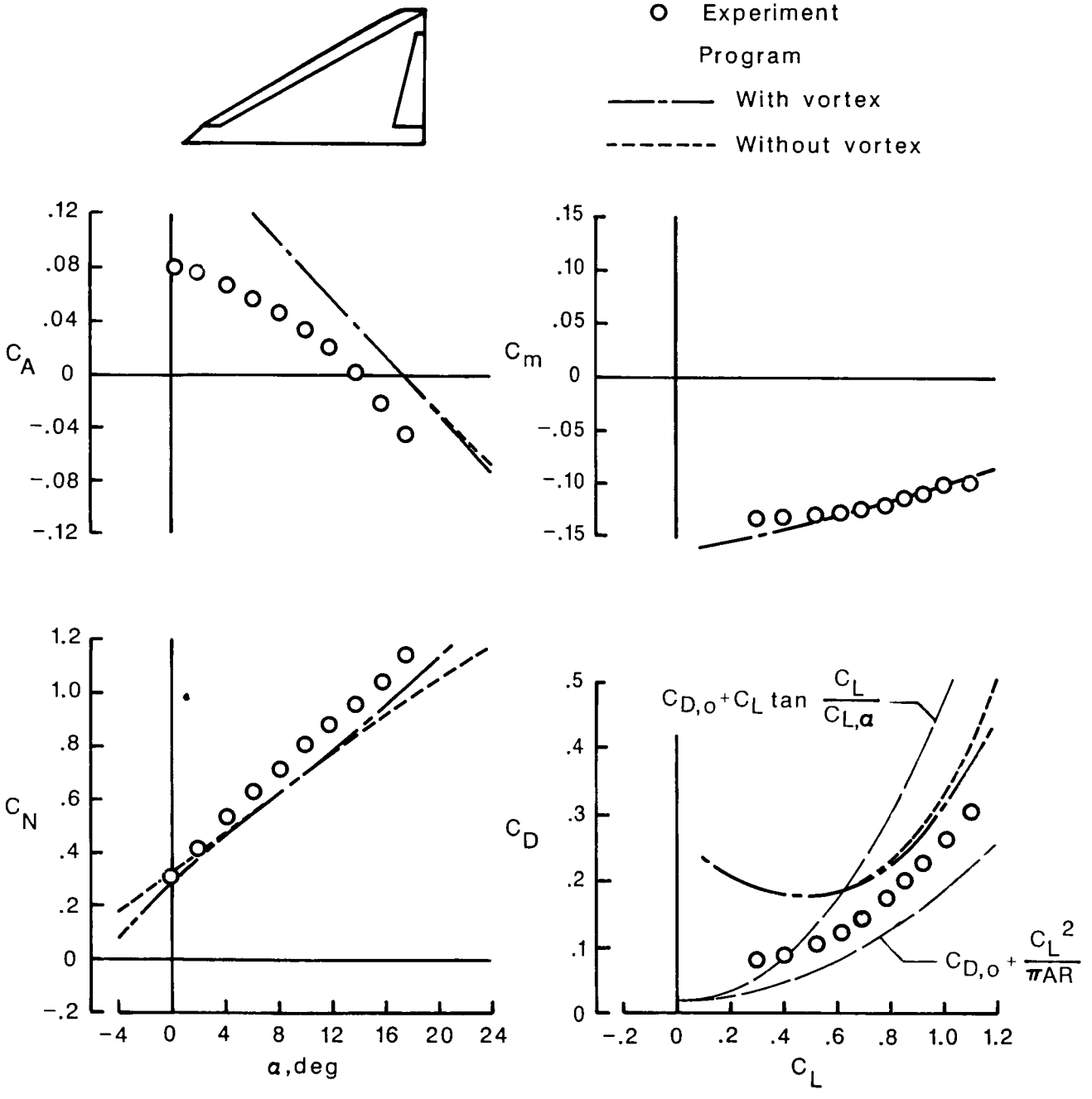

(c) $\delta_{L,n} = 60°$, $\delta_{T,n} = 30°$.

Figure 3. Concluded.

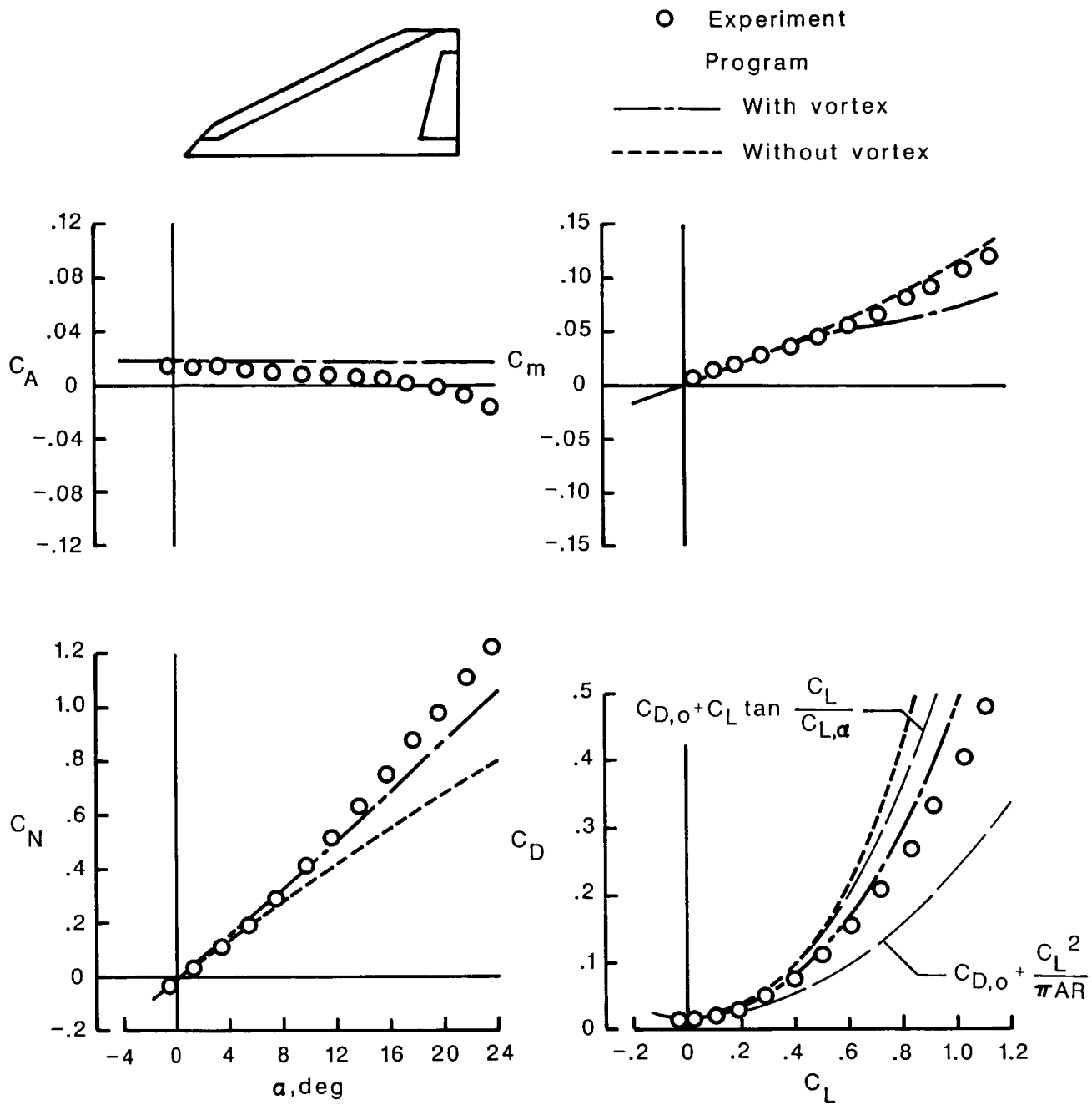

(a) $\delta_{L,n} = 0°$, $\delta_{T,n} = 0°$.

Figure 4. Comparison of program results and experimental data for 65°-swept cropped delta wing.

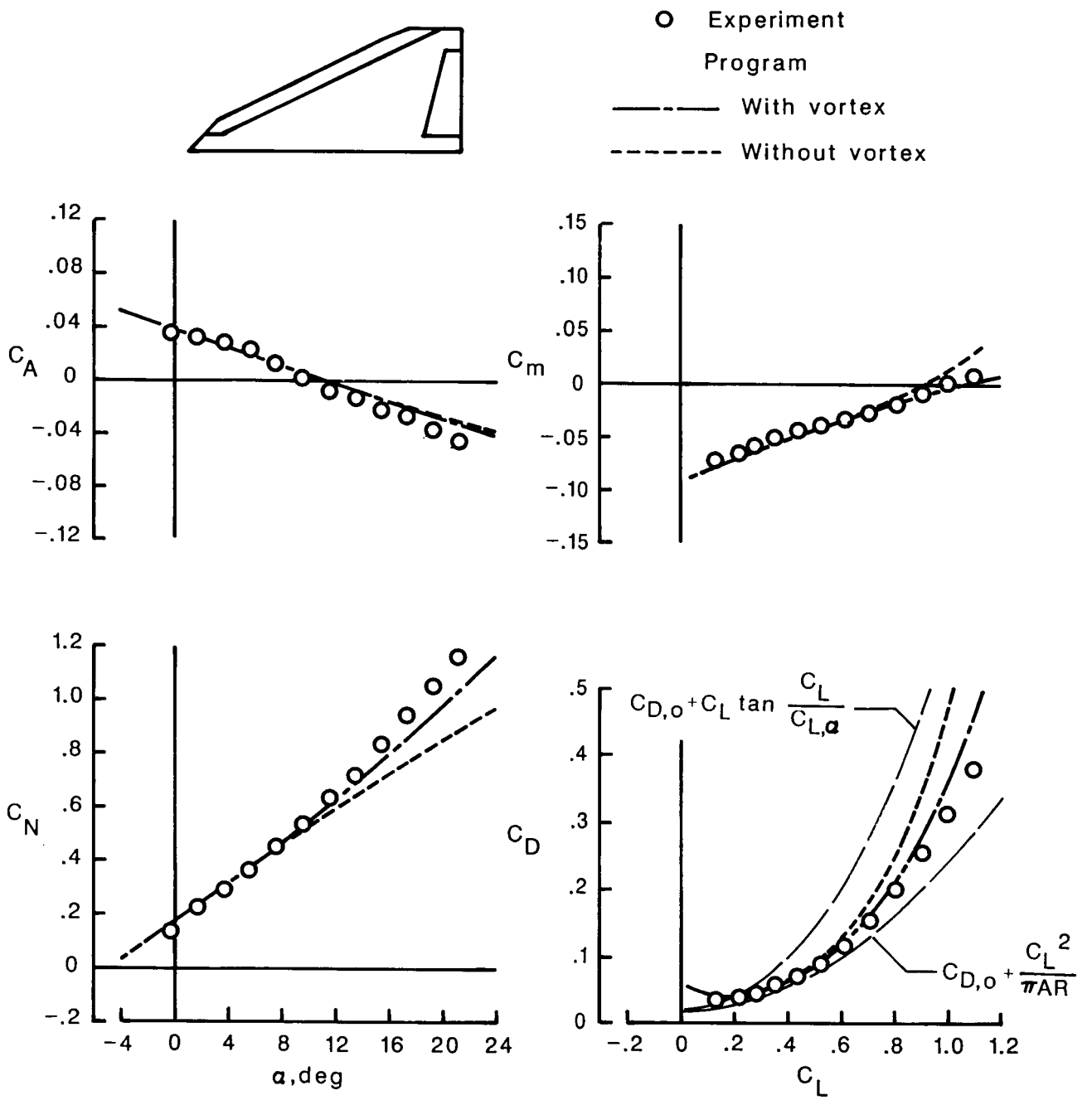

(b) $\delta_{L,n} = 30°$, $\delta_{T,n} = 15°$.

Figure 4. Continued.

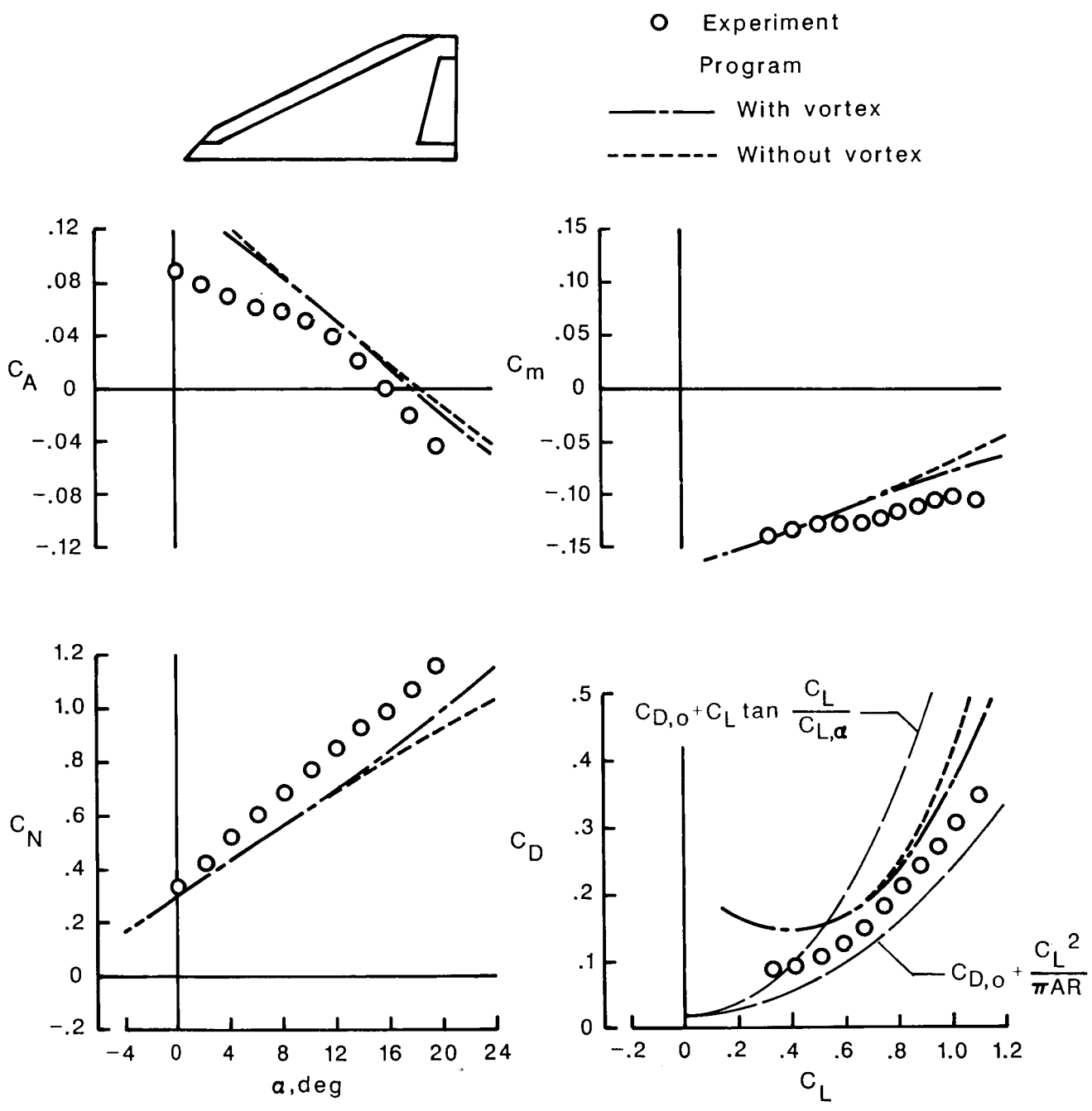

(c) $\delta_{L,n} = 60°$, $\delta_{T,n} = 30°$.

Figure 4. Concluded.

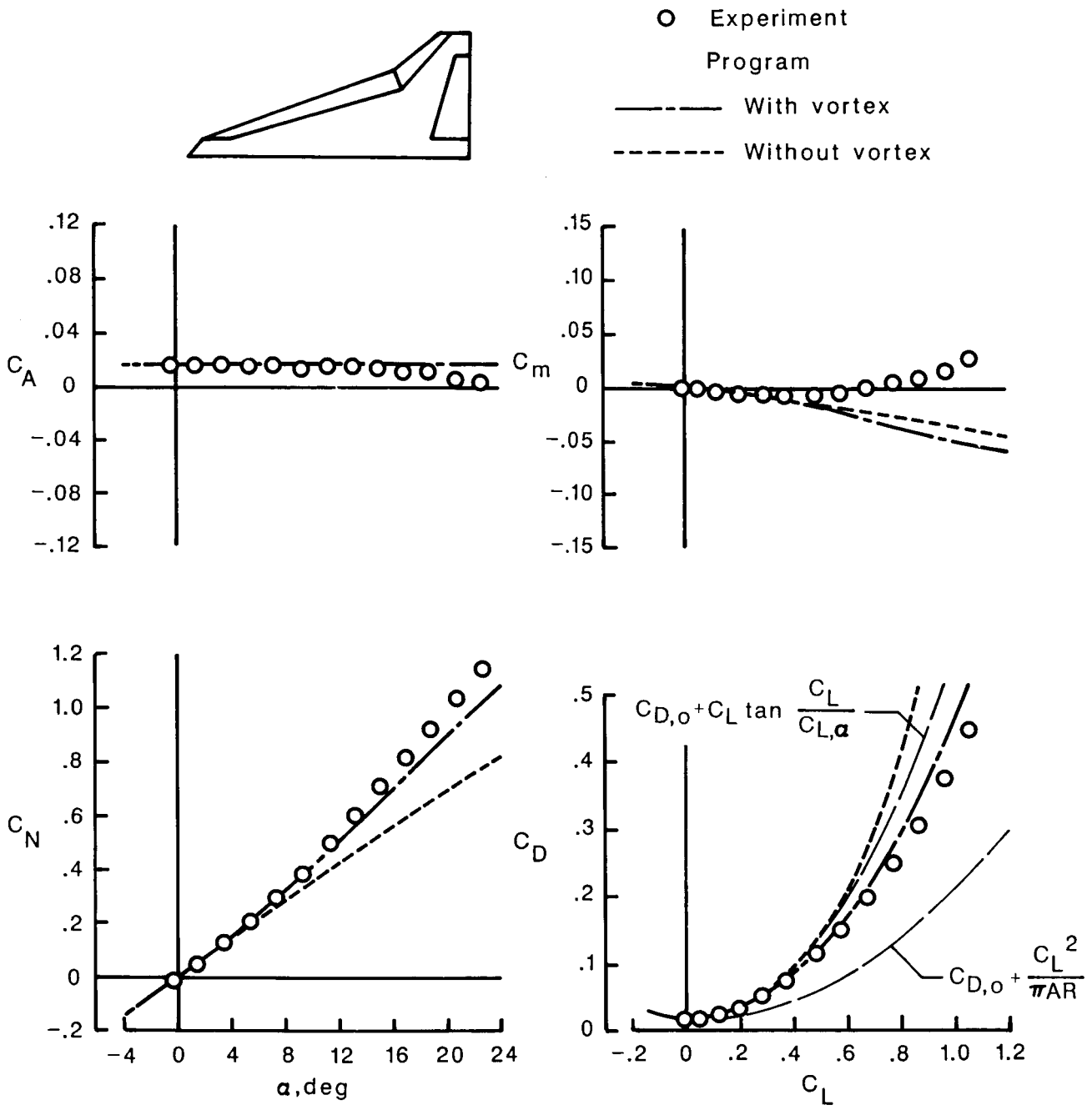

(a) $\delta_{L,n} = 0°$, $\delta_{T,n} = 0°$.

Figure 5. Comparison of program results and experimental data for 70°/50° cranked leading-edge wing.

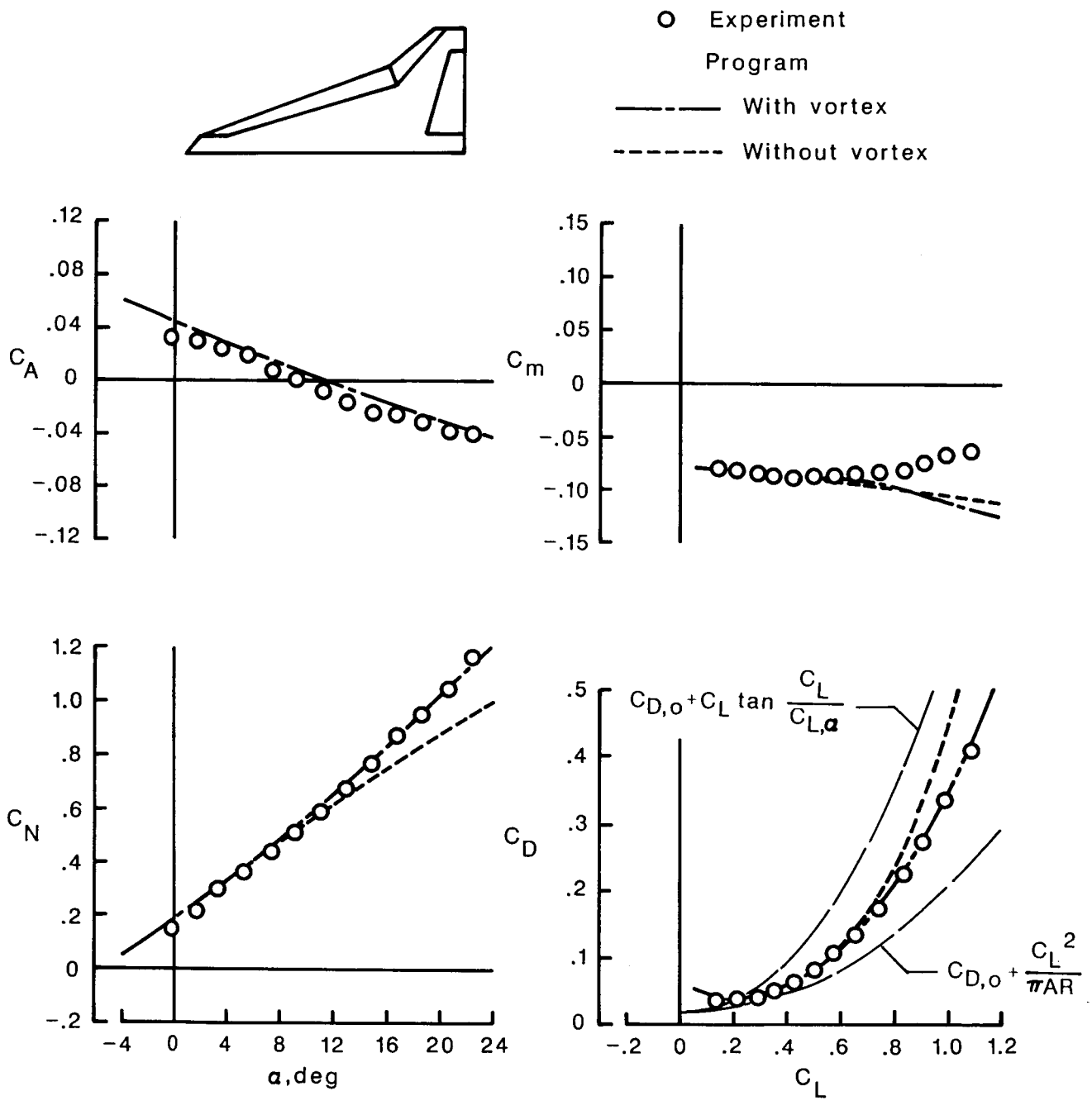

(b) $\delta_{L,n} = 30°$, $\delta_{T,n} = 15°$.

Figure 5. Concluded.

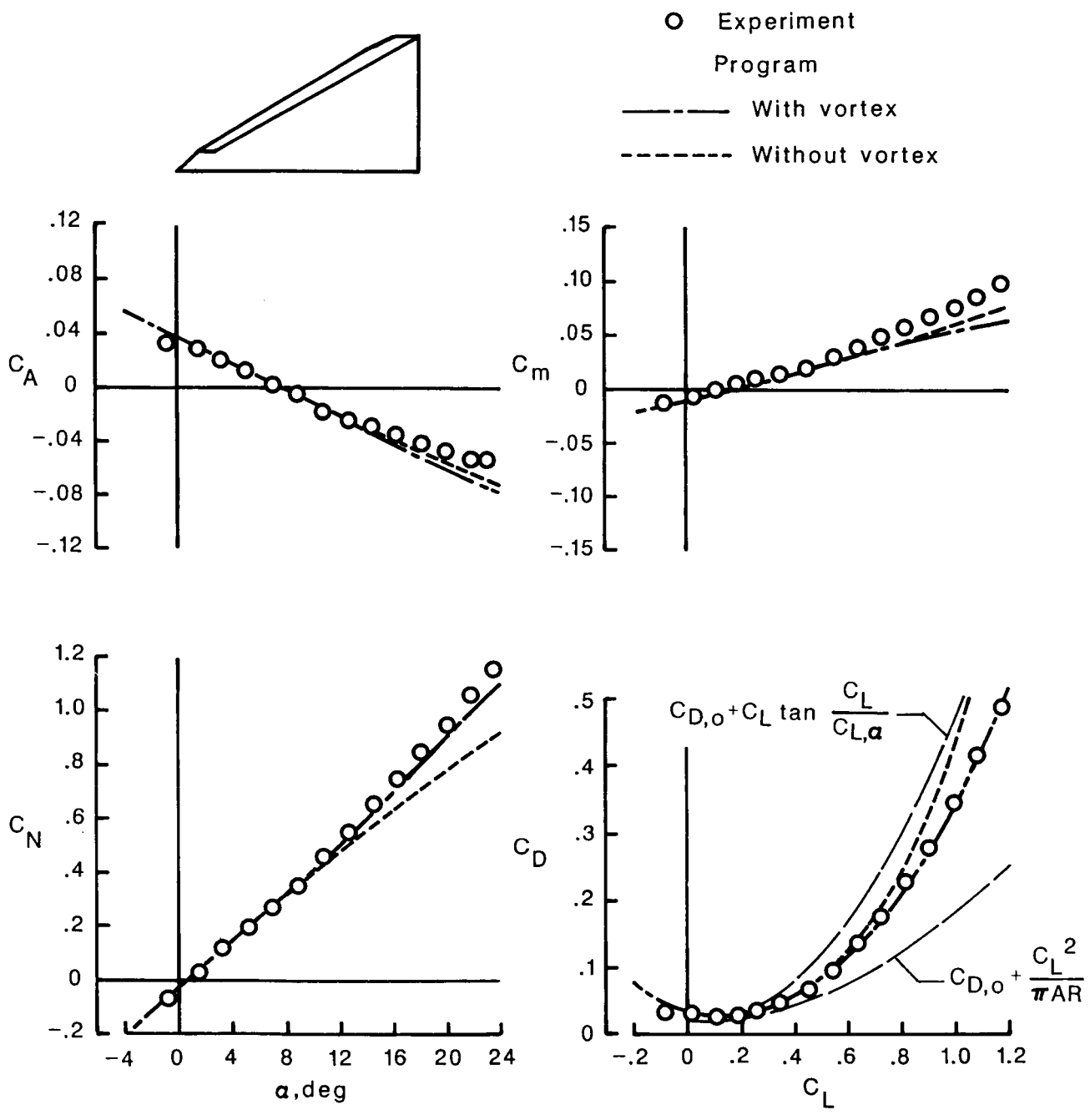

(a) Vortex leading-edge flap.

Figure 6. Comparison of program results and experimental data for 60°-swept cropped delta wing with two leading-edge flap planforms.

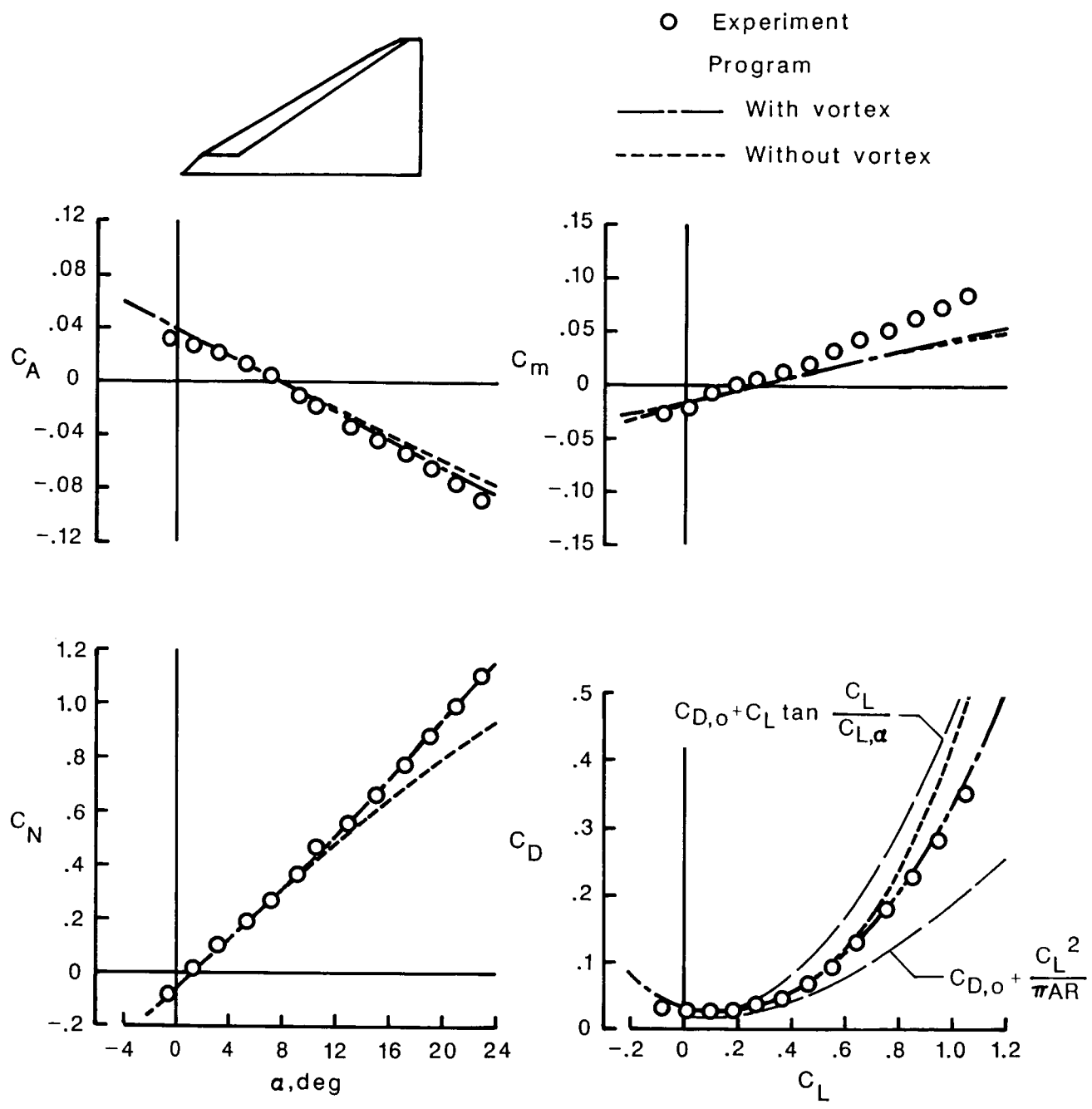

(b) Tapered leading-edge flap.

Figure 6. Concluded.

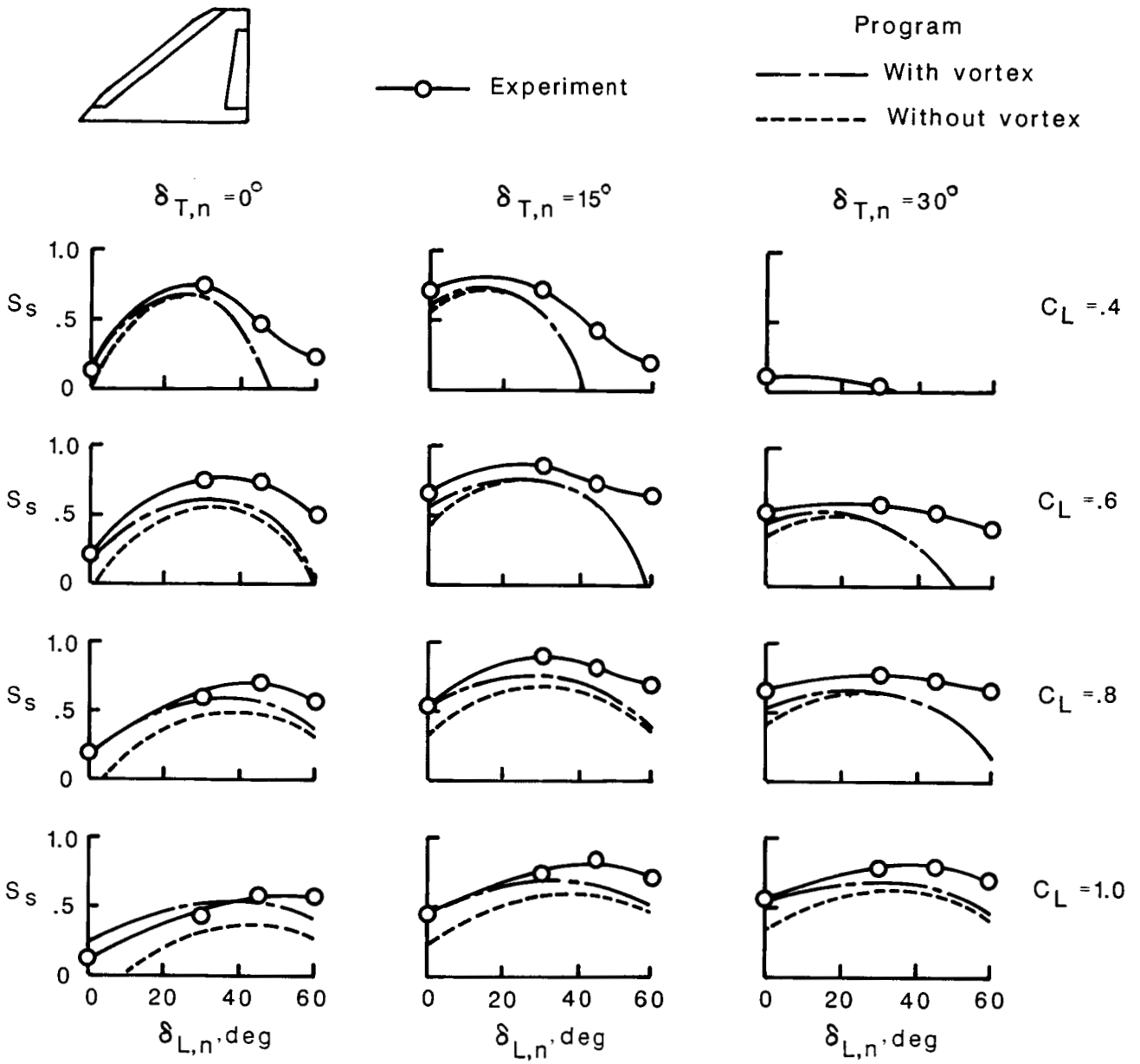

(a) 50°-swept cropped delta wing.

Figure 7. Variation of suction parameter with flap deflections for selected lift coefficients.

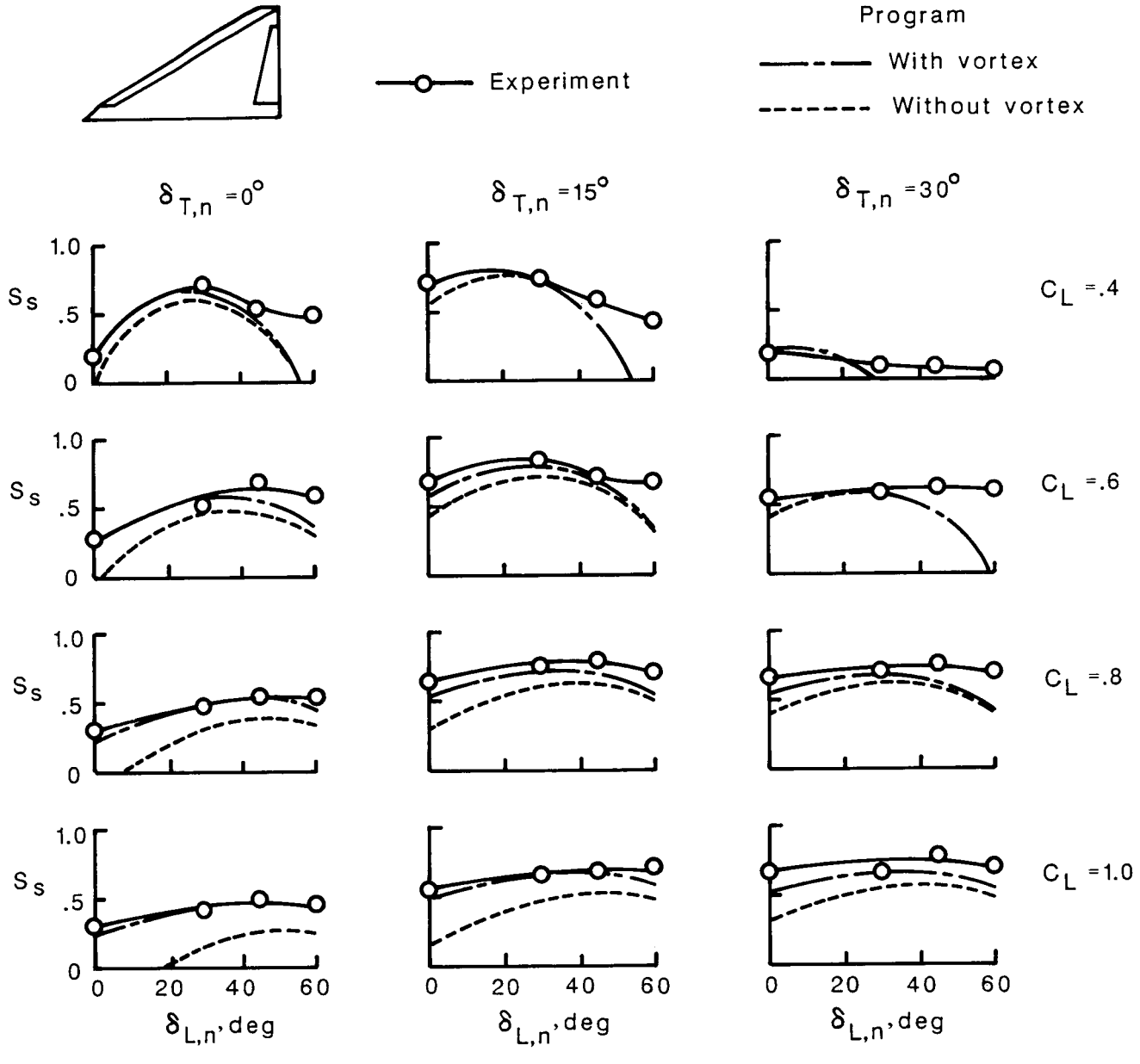

(b) 60°-swept cropped delta wing.

Figure 7. Continued.

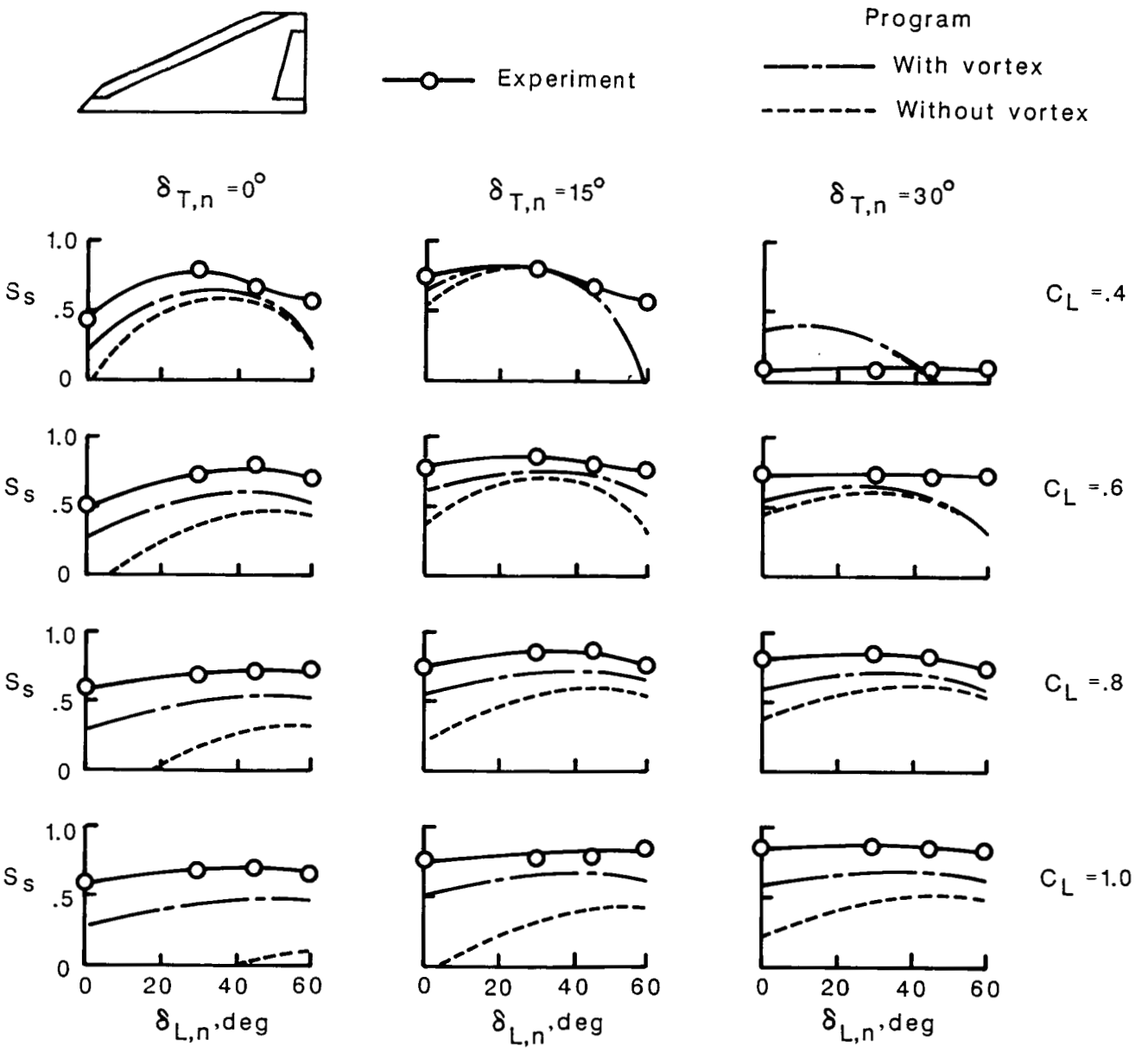

(c) 65°-swept cropped delta wing.

Figure 7. Continued.

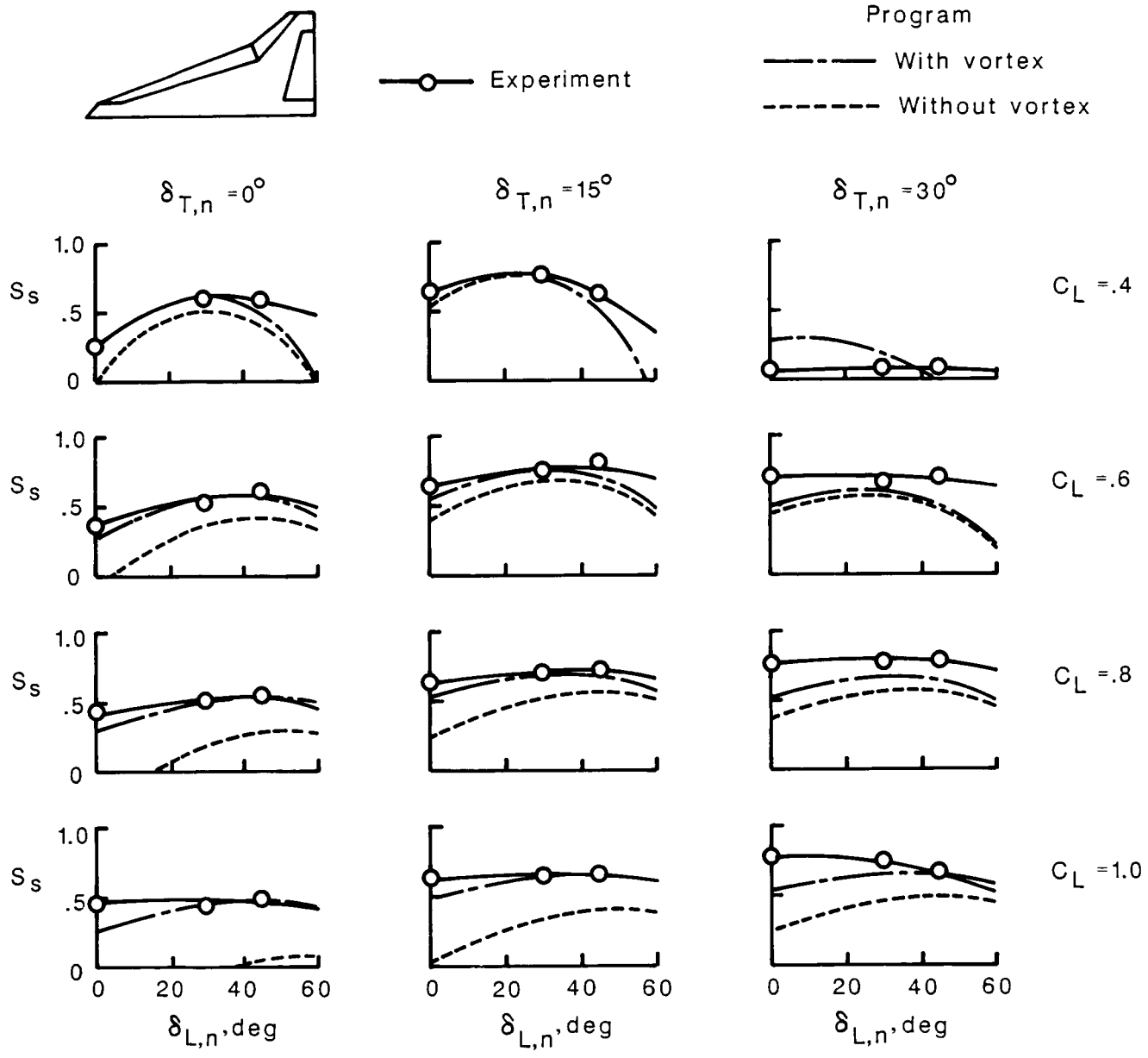

(d) 70°/50° cranked leading-edge wing.

Figure 7. Concluded.

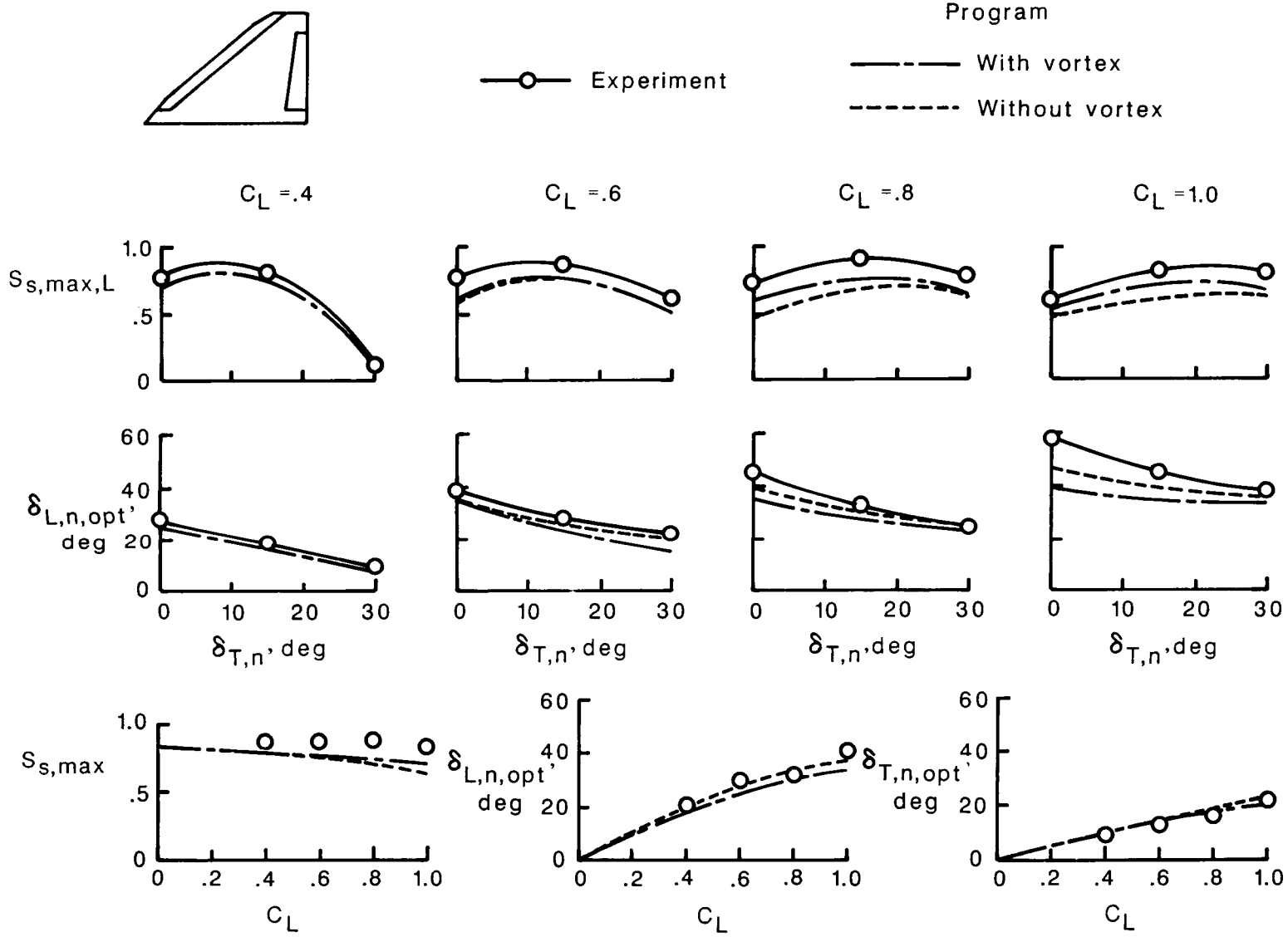

(a) 50°-swept cropped delta wing.

Figure 8. Maximum suction parameters and optimum flap deflections.

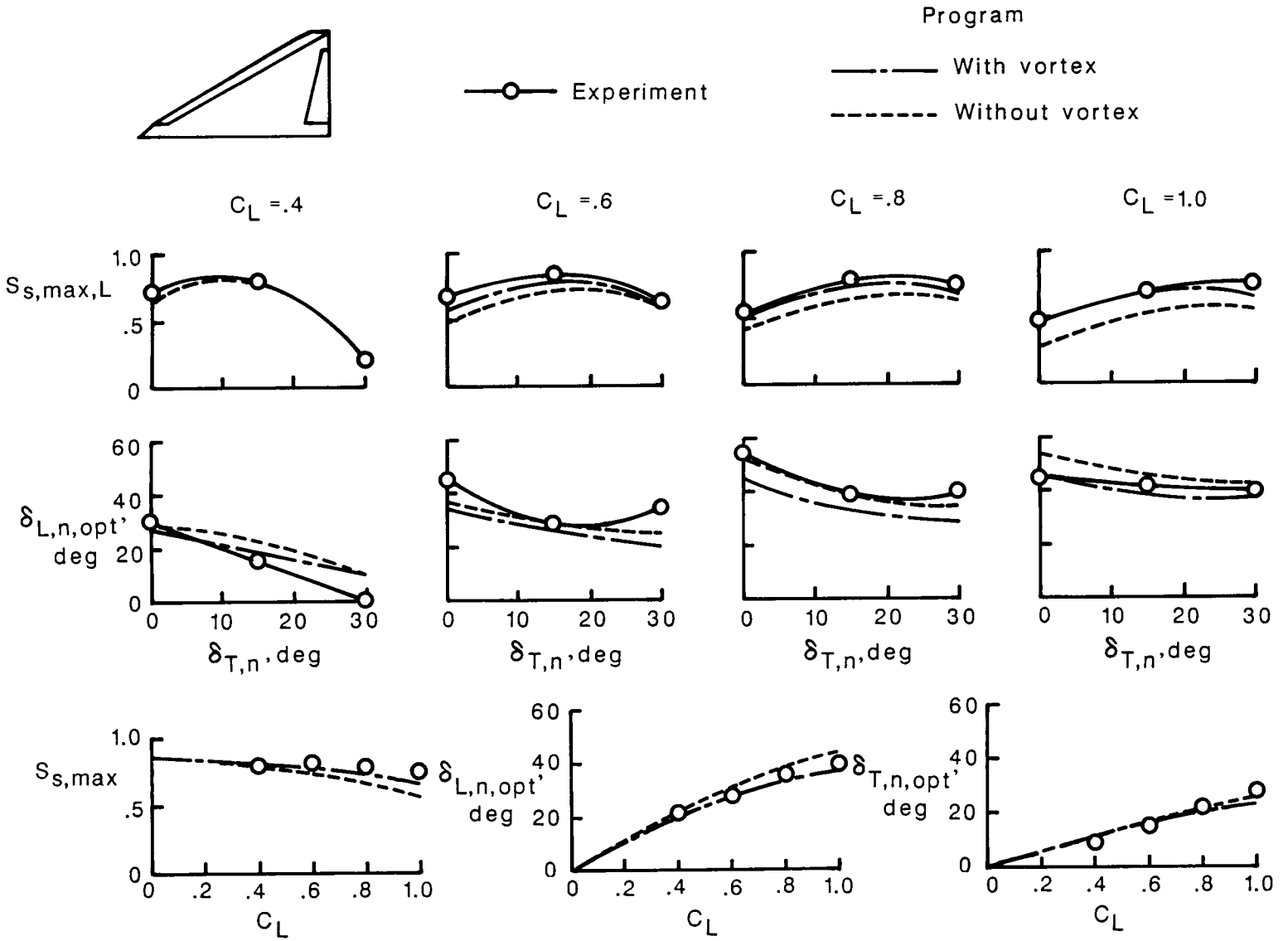

(b) 60°-swept cropped delta wing.

Figure 8. Continued.

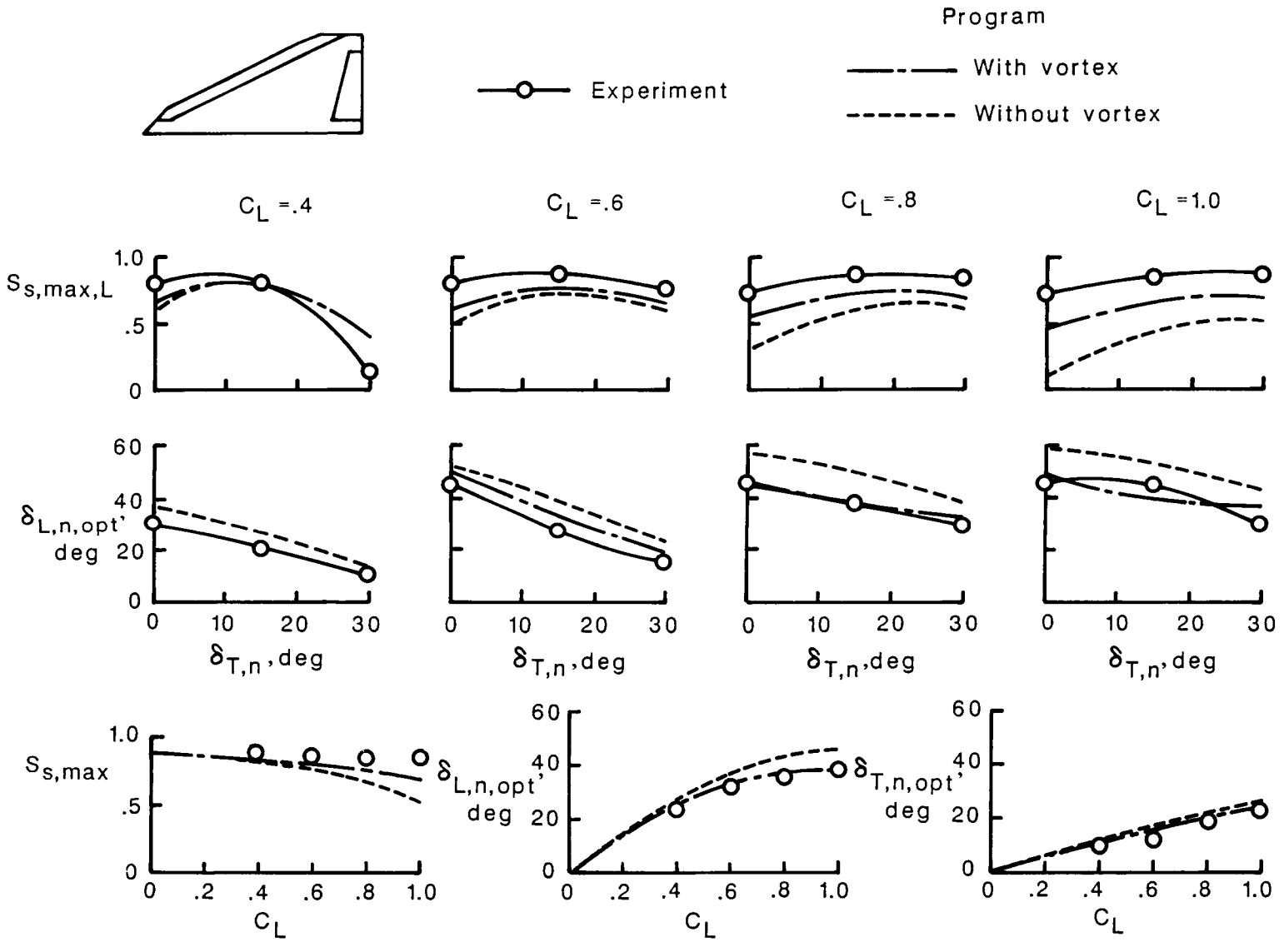

(c) 65°-swept cropped delta wing.

Figure 8. Continued.

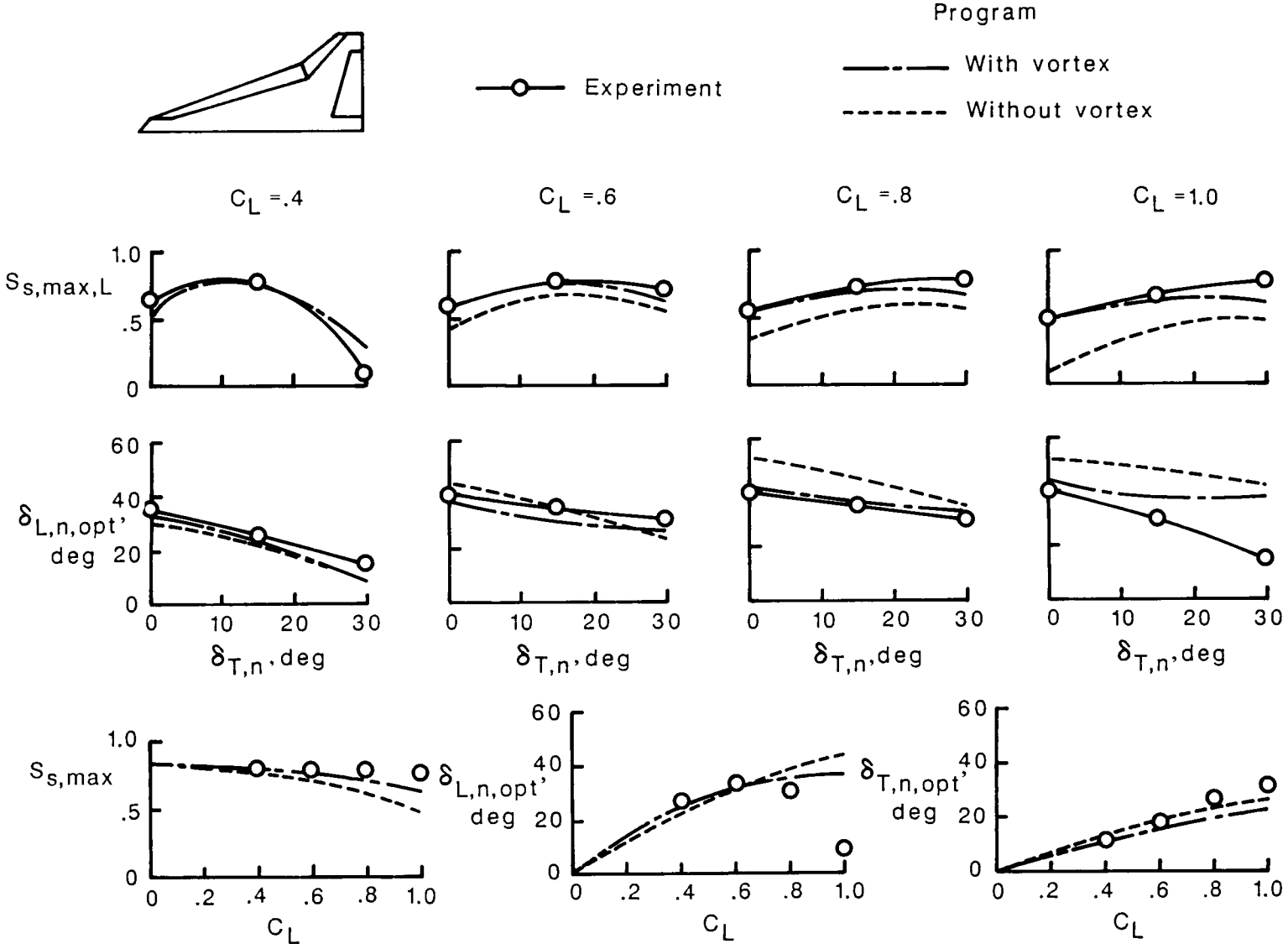

(d) 70°/50° cranked leading-edge wing.

Figure 8. Concluded.

• Maximum suction parameter with C_m = 0.04 restraint

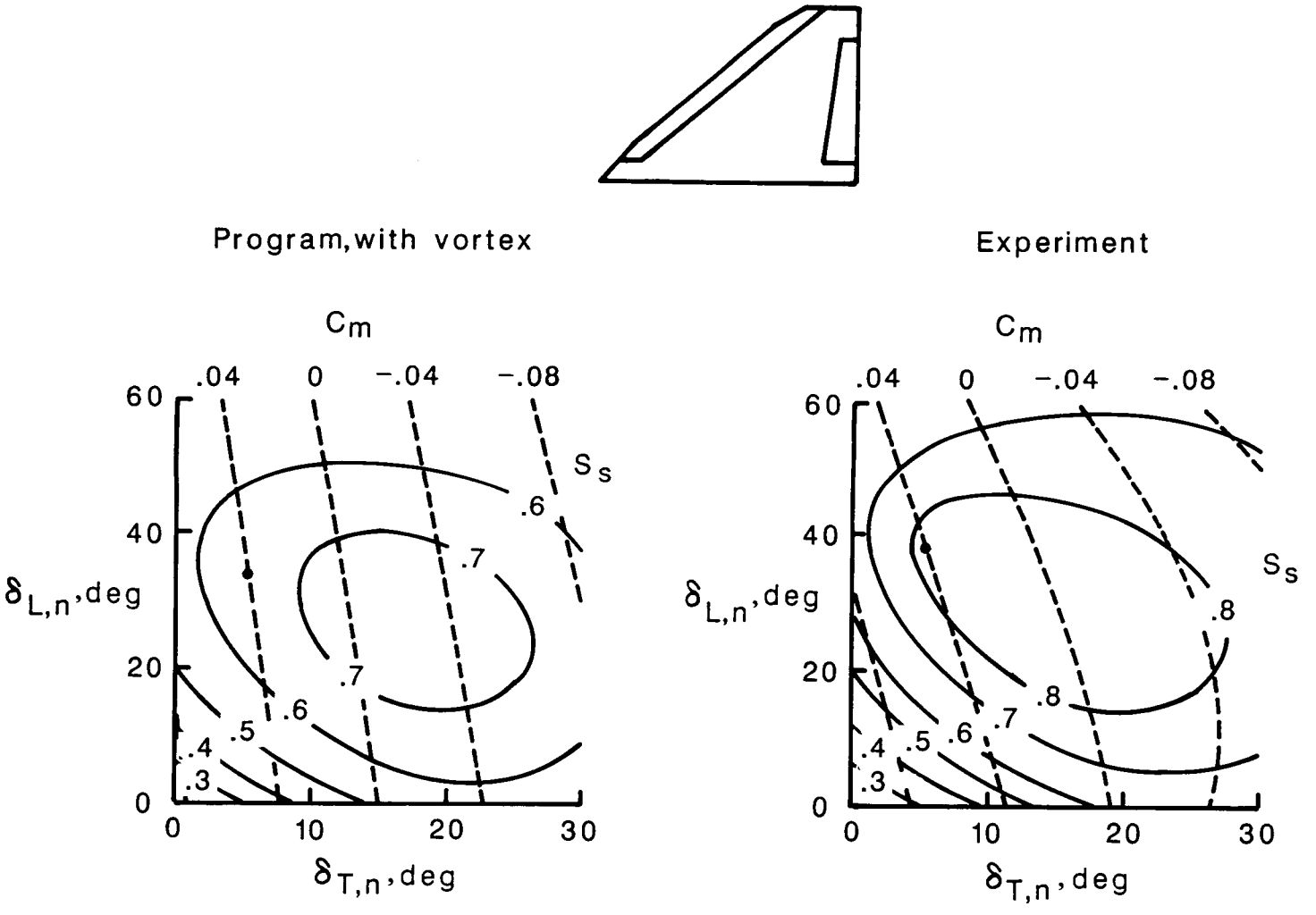

(a) 50°-swept cropped delta wing.

Figure 9. Sample flap-system performance maps for a lift coefficient of 0.8.

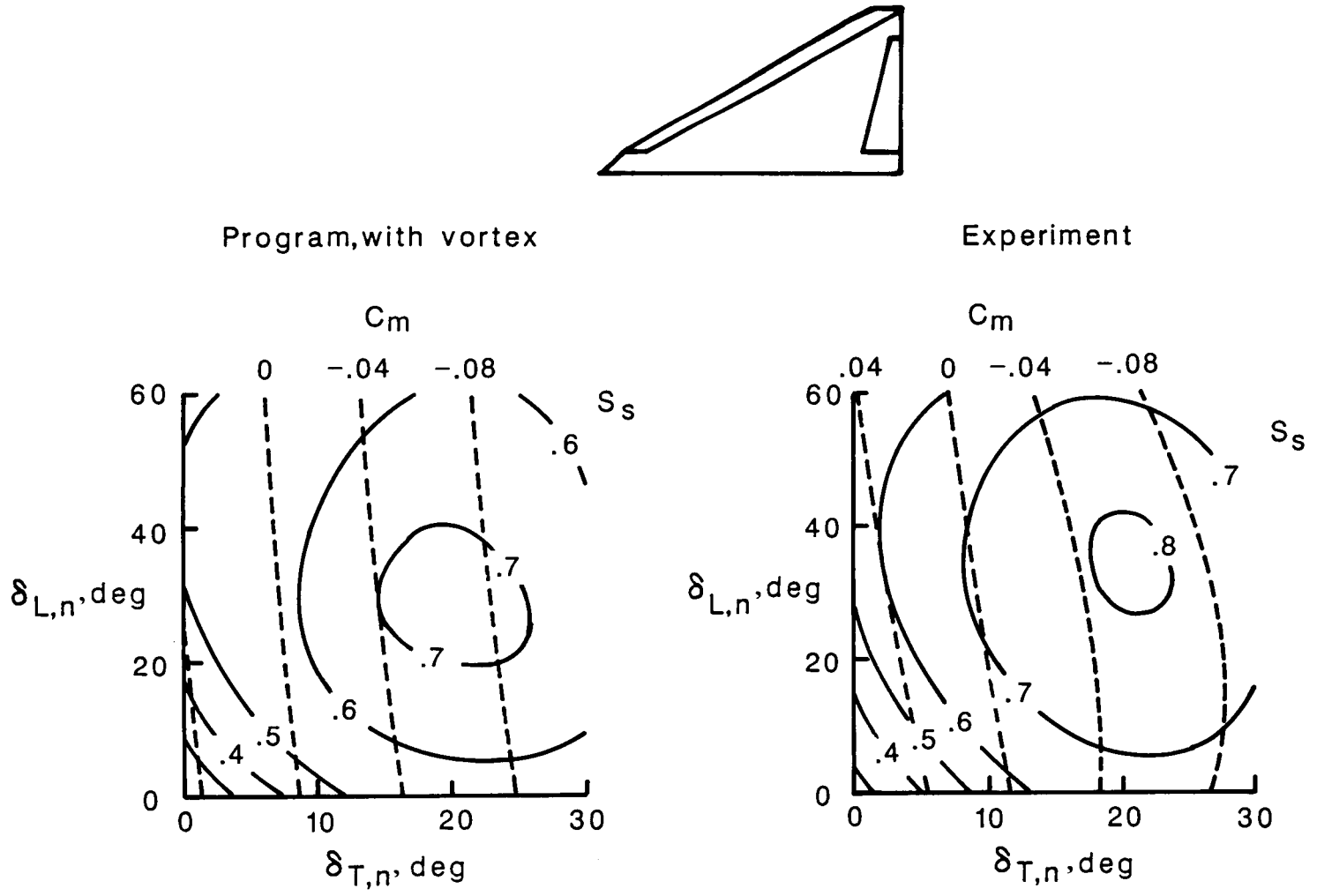

(b) 60°-swept cropped delta wing.

Figure 9. Continued.

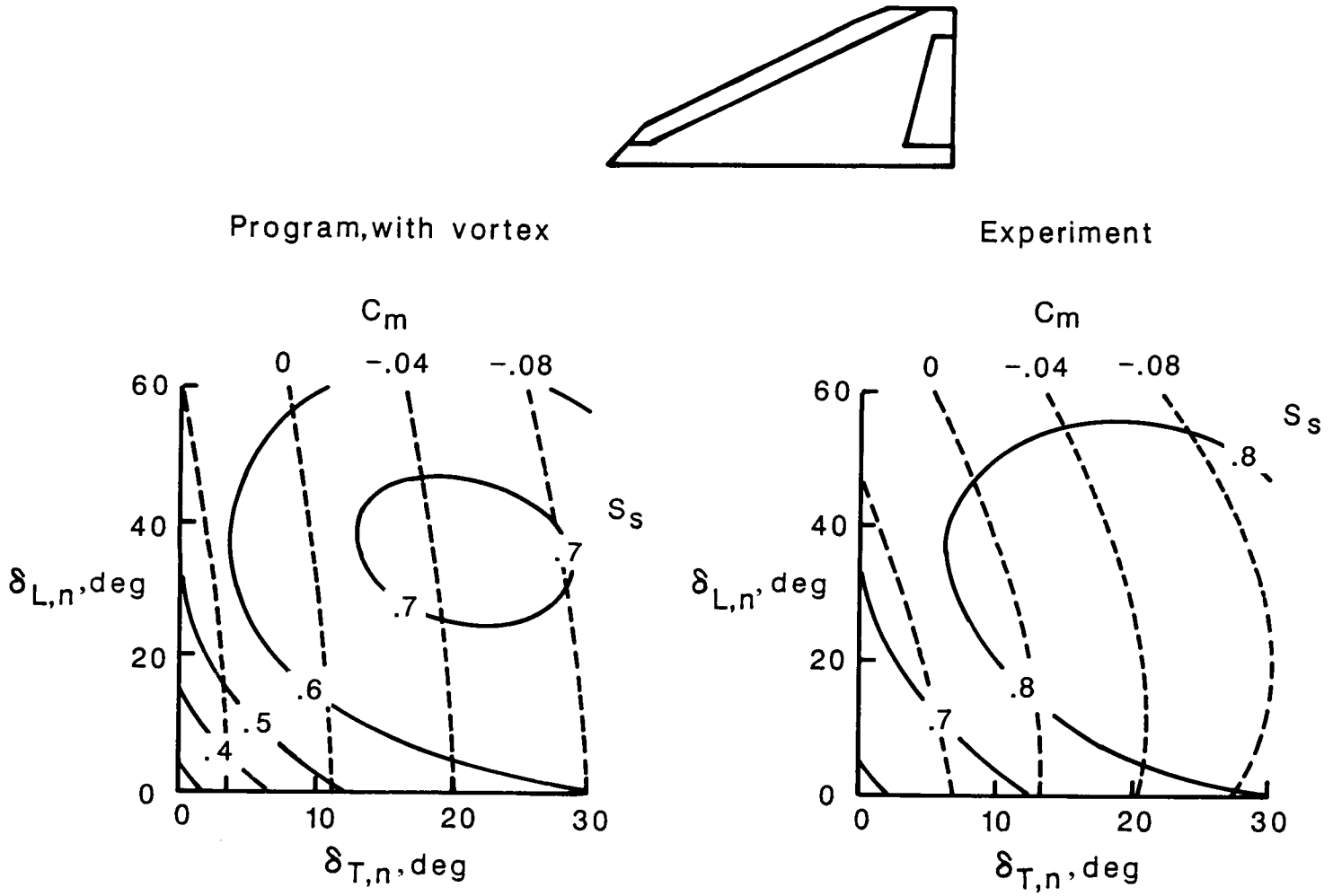

(c) 65°-swept cropped delta wing.

Figure 9. Continued.

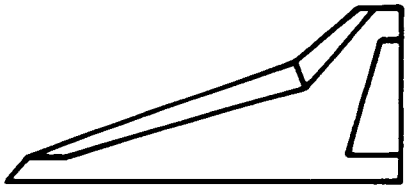

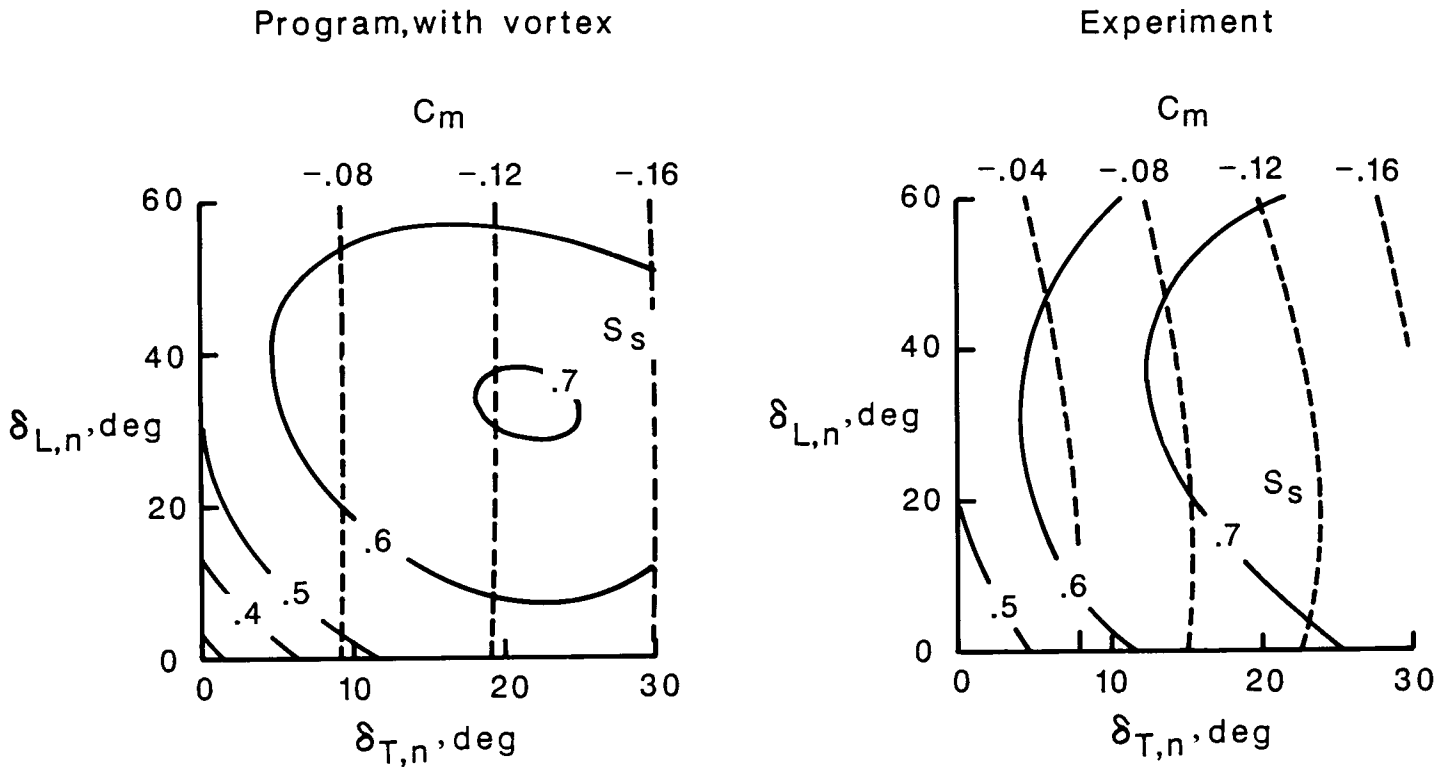

(d) 70°/50° cranked leading-edge wing.

Figure 9. Concluded.

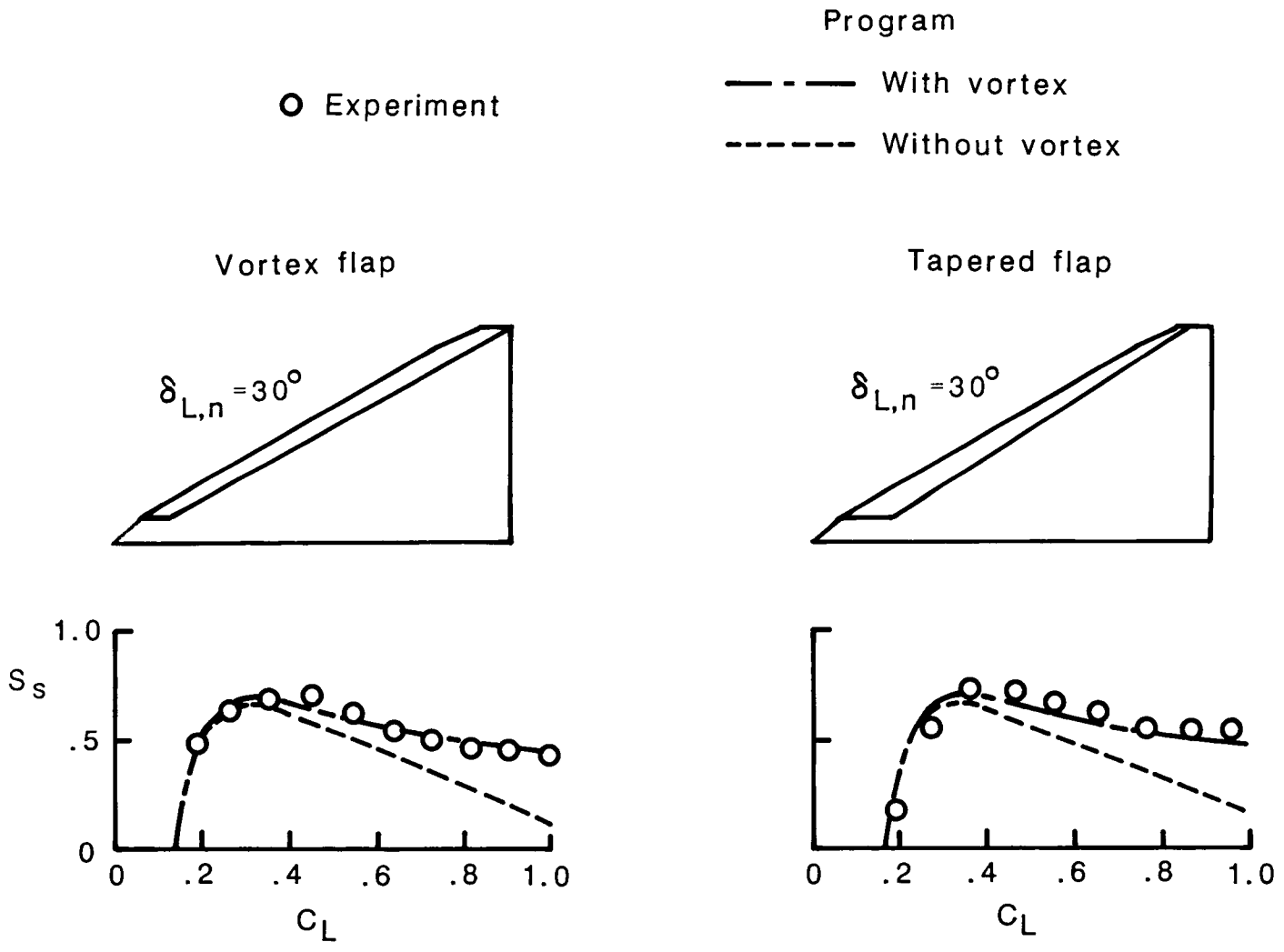

Figure 10. Comparison of performance of two leading-edge flap planforms for 60°-swept cropped delta wing.

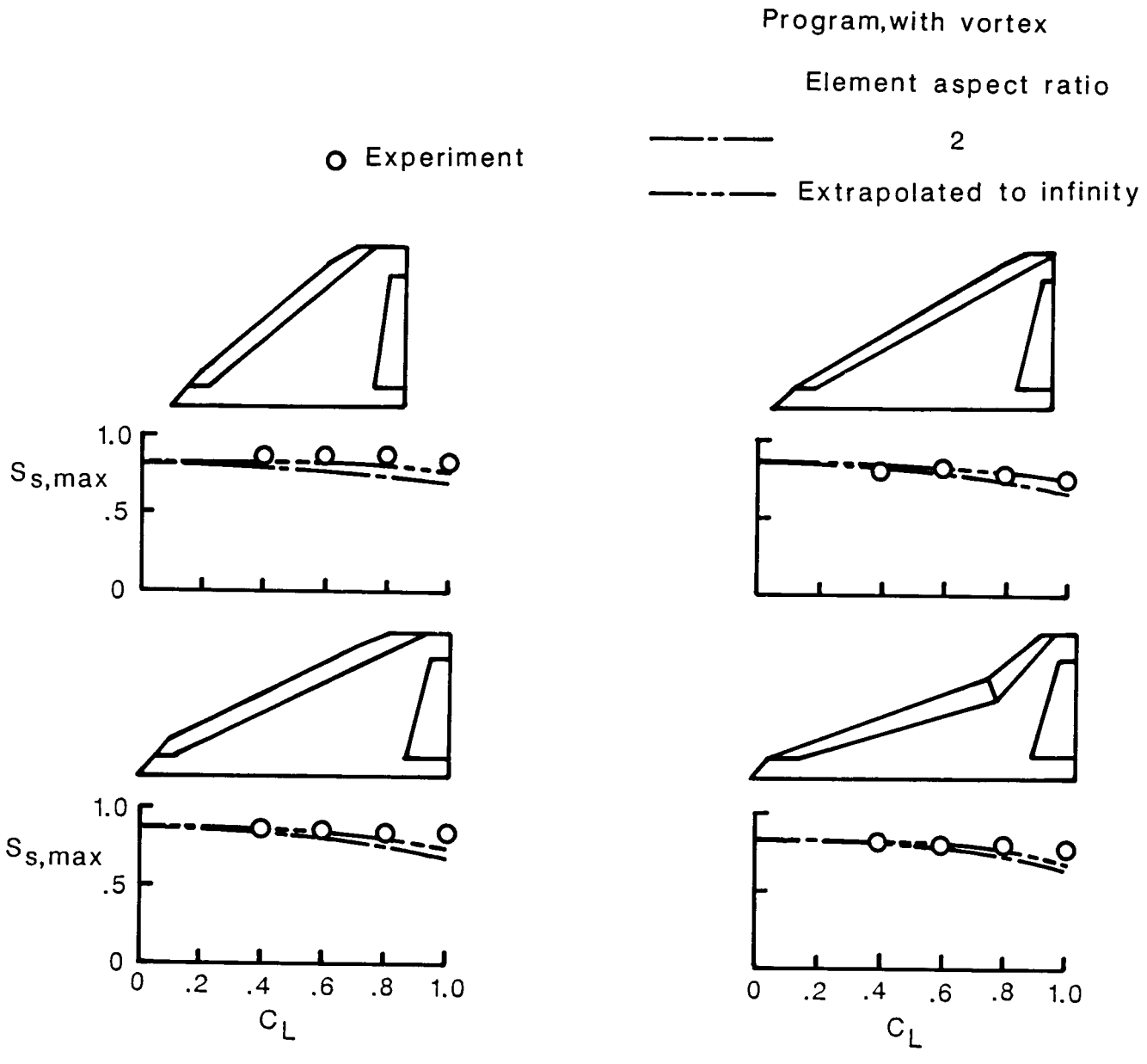

Figure 11. Suction parameters given by program with nominal element aspect ratio compared with extrapolated values.

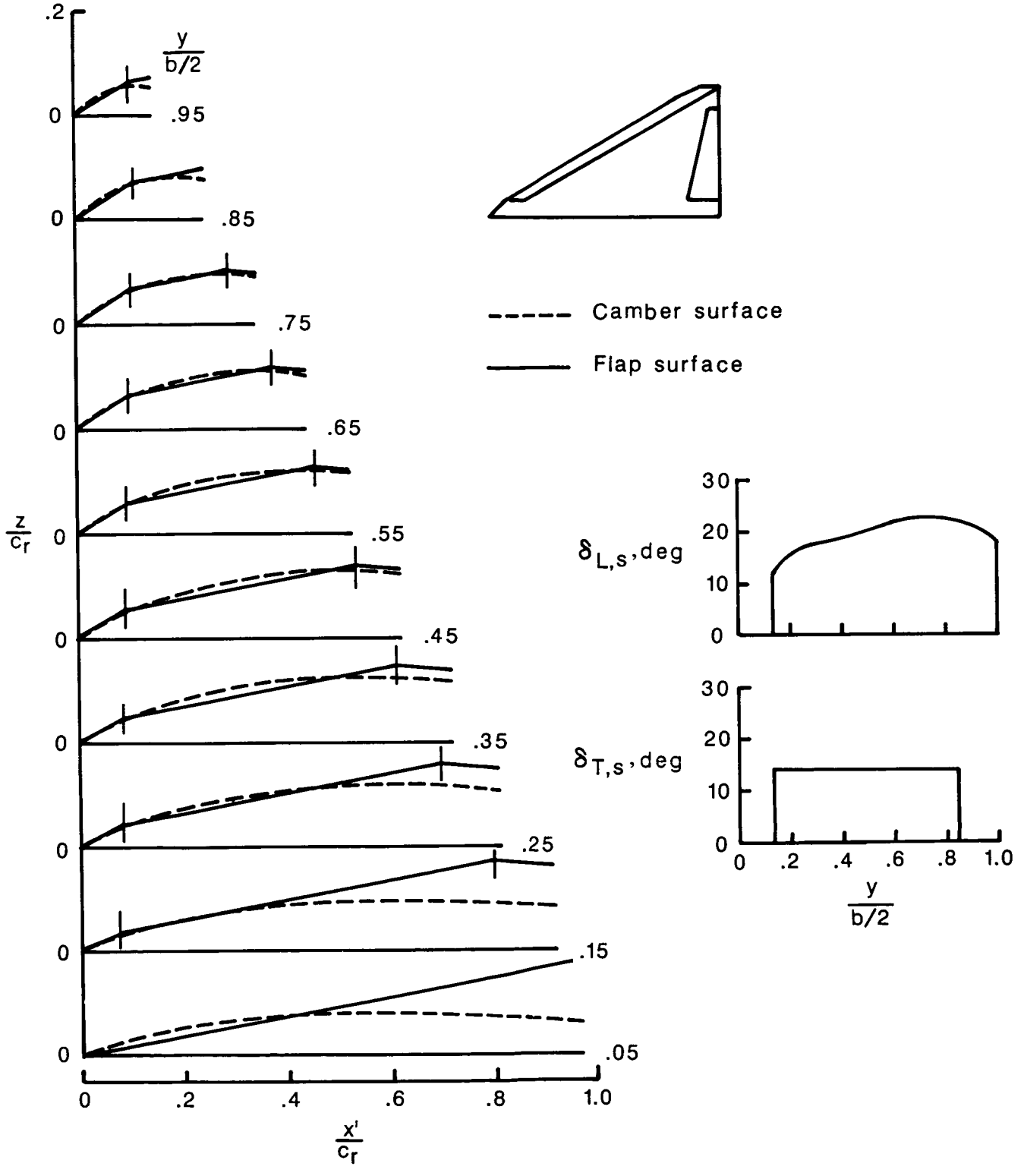

Figure 12. Wing-design program camber surface for 60°-swept cropped delta wing at a design lift coefficient of 0.70.

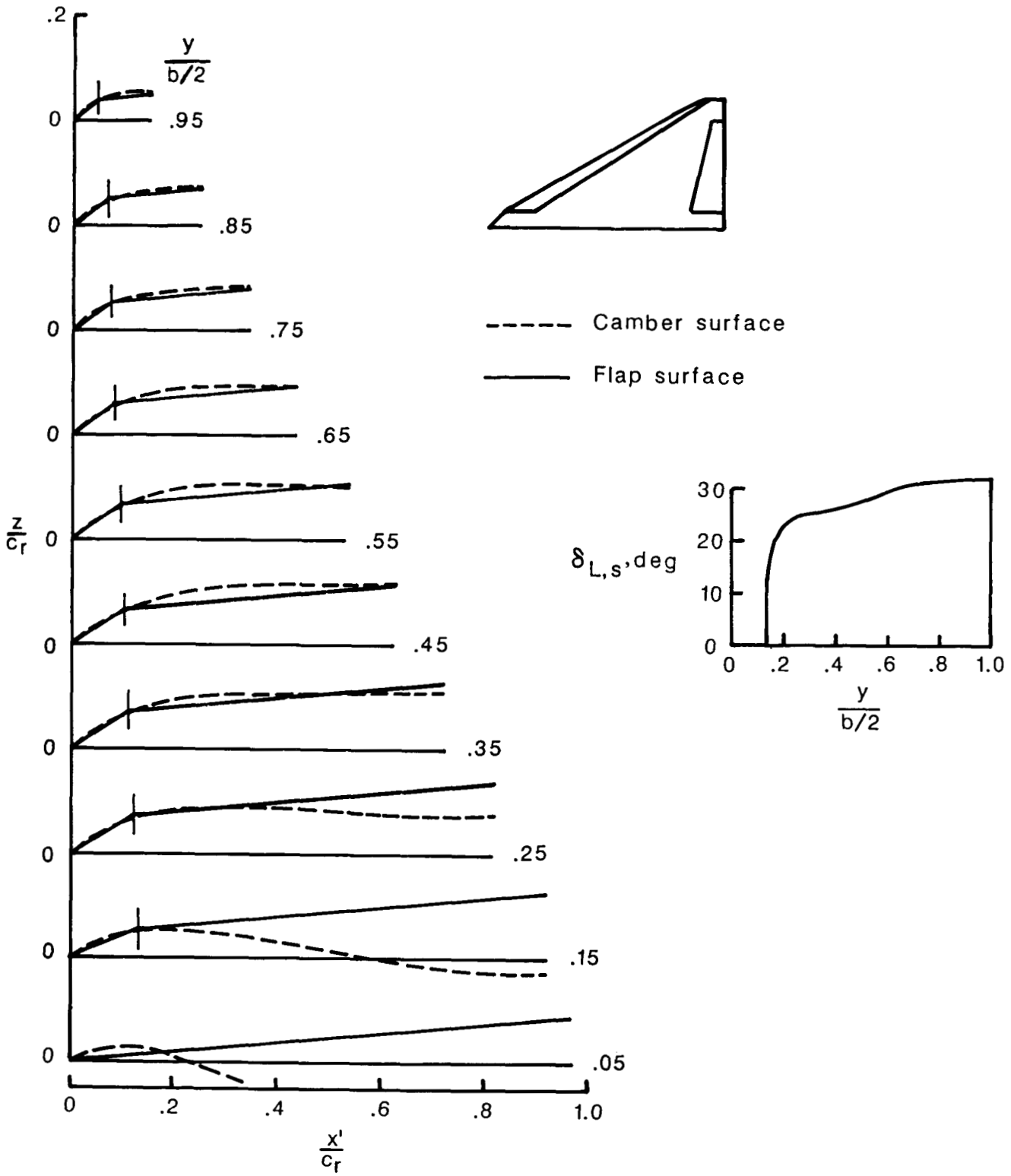

Figure 13. Wing-design program restricted-area camber surface for 60°-swept cropped delta wing at a design lift coefficient of 0.70 and a design moment coefficient of −0.05.

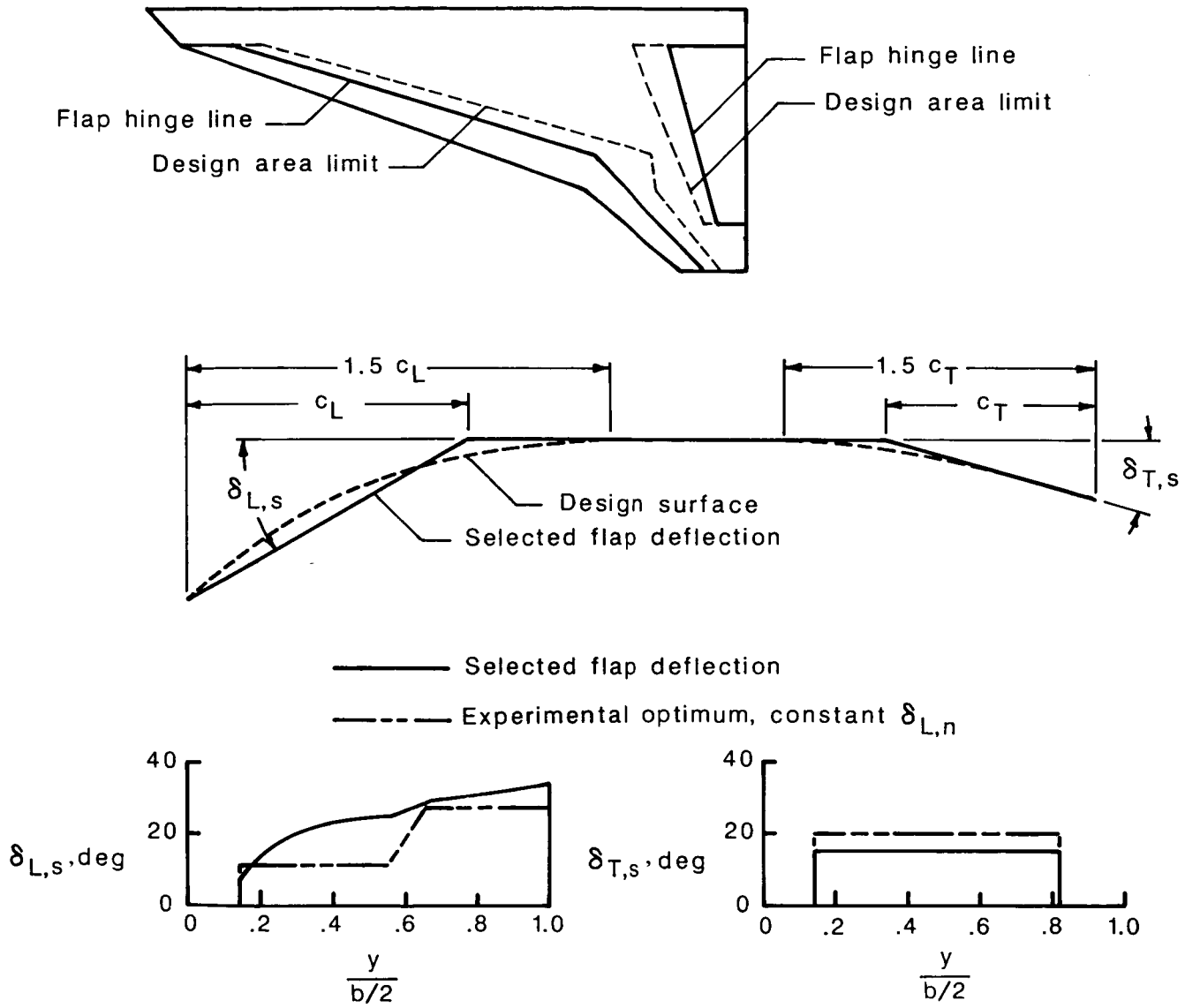

Figure 14. Wing-design program restricted-area camber surface for 70°/50° cranked leading-edge wing at a design lift coefficient of 0.7 and a design moment coefficient of −0.12.

Standard Bibliographic Page

1. Report No.	2. Government Accession No.	3. Recipient's Catalog No.
NASA TP-2653		

4. Title and Subtitle	5. Report Date
Applicability of Linearized-Theory Attached-Flow Methods to Design and Analysis of Flap Systems at Low Speeds for Thin Swept Wings With Sharp Leading Edges	January 1987
	6. Performing Organization Code: 505-62-81-01
7. Author(s): Harry W. Carlson and Christine M. Darden	8. Performing Organization Report No.: L-16151
9. Performing Organization Name and Address: NASA Langley Research Center, Hampton, VA 23665-5225	10. Work Unit No.
	11. Contract or Grant No.
12. Sponsoring Agency Name and Address: National Aeronautics and Space Administration, Washington, DC 20546-0001	13. Type of Report and Period Covered: Technical Paper
	14. Sponsoring Agency Code

15. Supplementary Notes

Harry W. Carlson: PRC Kentron, Inc., Hampton, Virginia.
Christine M. Darden: Langley Research Center, Hampton, Virginia.

16. Abstract

Low-speed experimental force and data on a series of thin swept wings with sharp leading edges and leading- and trailing-edge flaps are compared with predictions made using a linearized-theory method which includes estimates of vortex forces. These comparisons were made to assess the effectiveness of linearized-theory methods for use in the design and analysis of flap systems in subsonic flow. Results demonstrate that linearized-theory, attached-flow methods (with approximate representation of vortex forces) can form the basis of a rational system for flap design and analysis. Even attached-flow methods that do not take vortex forces into account can be used for the selection of optimized flap-system geometry, but design-point performance levels tend to be underestimated unless vortex forces are included. Illustrative examples of the use of these methods in the design of efficient low-speed flap systems are included.

17. Key Words (Suggested by Authors(s))	18. Distribution Statement
Aerodynamics Numerical methods Flap systems Vortex flaps Linearized theory	Unclassified—Unlimited Subject Category 02

19. Security Classif.(of this report)	20. Security Classif.(of this page)	21. No. of Pages	22. Price
Unclassified	Unclassified	52	A04

For sale by the National Technical Information Service, Springfield, Virginia 22161

NASA-Langley, 1987